SEMIANNUAL PROGRESS REPORT

October, 1976 - March, 1976

Flight Test Evaluation of a Method to Determine the Level Flight Performance of Propeller - Driven Aircraft

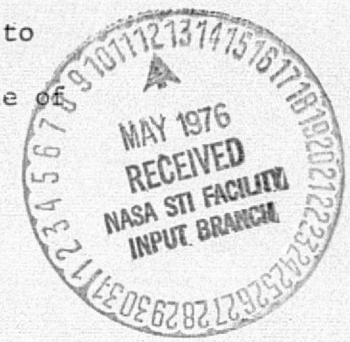

NASA Grant Number NSG 1231

Principal Investigator

Ernest J. Cross, Jr., Ph.D.
Professor and Director
of the Raspet Flight
Research Laboratory

Mississippi State University
Department of Aerophysics and Aerospace Engineering
Mississippi State, Mississippi 39762

Program progress is essentially on schedule. The following sections provide a detailed commentary on the supporting theory of the method, instrumentation, flight test procedure, and data and analyses. The flight test schedule is not yet complete, however, sufficient data have been generated to indicate quite good potential for the method. Subsequent flights will be to investigate additional drogues of higher drag and another propeller to provide comparative data covering a wider spectrum of propeller performance.

A procedure has been developed for deriving the level flight drag and propulsive efficiency of propeller-driven aircraft. This is a method in which the overall drag of the aircraft is expressed in terms of the measured increment of power required to overcome a corresponding known increment of drag. The aircraft is flown in unaccelerated, straight and level flight, and thus includes the effects of the propeller drag and slipstream. Propeller efficiency and airplane drag are computed on the basis of data obtained during flight test and do not rely on the analytical calculations of inadequate theory.

The propulsive efficiency of a propeller driven aircraft is defined as

$$\eta_p = \frac{THP}{SHP} = \frac{TV}{SHP} \qquad (1)$$

where η_p is the propulsive efficiency, T is the net thrust acting on the airplane, V is its true velocity, and SHP is the power delivered to the propeller.

In unaccelerated, straight and level flight, the thrust can be expressed in terms of the drag D and the thrust inclination angle γ (Fig. 1) such that $T = D/\cos\gamma$. At normal flight speeds, the thrust inclination

angle is small and the approximation is made that cos $\gamma = 1$. Then $T = D$ and

$$\eta_p = \frac{DV}{SHP} \tag{2}$$

When an increment of drag ΔD is added to the aircraft and a corresponding amount of power ΔSHP is added to maintain the same airspeed and altitude, the propulsive efficiency equation becomes

$$\eta_p + \Delta\eta_p = \frac{(D + \Delta D)V}{SHP + \Delta SHP} \tag{3}$$

where $\Delta\eta_p$ is the change in propulsion efficiency caused by the change in power.

The drag D can be eliminated from equation (3) by use of equation (2). Making the substitution gives

$$\eta_p = \frac{\Delta DV}{\Delta SHP} - \frac{\Delta\eta_p\ (SHP + \Delta SHP)}{\Delta SHP} \tag{4}$$

A propulsive efficiency ratio can be defined as

$$E_p = \frac{\eta_p + \Delta\eta_p}{\eta_p} = 1 + \frac{\Delta\eta_p}{\eta_p} \tag{5}$$

Equation (4) can then be written as

$$\eta_p = \frac{\Delta DV}{(SHP + \Delta SHP)\ E_p - SHP} \tag{6}$$

Substituting this equation into equation (2) gives the basic incremental drag equation.

$$D = \frac{\Delta D}{(1 + \frac{\Delta SHP}{SHP})E_p - 1} \tag{7}$$

If the propulsive efficiency remains a constant, then $E_p = 1$ and a special case of the incremental drag equation is obtained where

$$D = \Delta D\ \frac{SHP}{\Delta SHP} \tag{8}$$

This equation is of great interest to the researcher. All the parameters on the right side of the equation can be easily measured. The drag

of the aircraft can then be obtained without the use of a propeller efficiency chart or uncertain theoretical calculations. And after finding the drag, the propeller efficiency can be calculated directly from equation (2).

The propeller efficiency does remain nearly constant for certain operating conditions. A plot (Fig. 2) of propeller efficiency versus coefficient of power with lines of constant advance ratio was prepared for a two-bladed propeller with an activity factor of ninety.

This is the same type of propeller on the test aircraft. The graph shows that for the higher advance ratios ($J \geq .6$), the propeller efficiency is relatively insensitive to small changes in power. Thus, a combination of high airspeeds and/or low propeller rpm will keep the efficiency change small. The aircraft velocity and propeller speed are maintained constant for each test point. Thus, the advance ratio J remains a constant for both of the power conditions SHP and SHP + ΔSHP at each test point. Only the associated coefficient of power C_p changes. Thus, for the test conditions described, the approximation of constant propeller efficiency is quite good.

Equation (7) can be used to compute aircraft drag if the assumption of constant propeller efficiency is not admissable. Figure (2) can then be used to calculate E_p, the propulsive efficiency ratio. Although the actual values of η_p on the chart are questionable, the relative change should be fairly accurate, since the data was obtained from wind tunnel tests on a propeller similar to that on the aircraft.

The derivation of the incremental drag equation has assumed that the only change in aircraft drag is due to the drag chute. The addition of the drag chute, however, could cause a change in the profile and induced drag

of the aircraft.

When the drag chute is attached to the tail, it generates a nose down pitching moment about the aircraft center-of-gravity. To counter this, the pilot must add an "up" elevator movement. The elevator trim tab will likely be changed to correct for the adverse stick force. These two changes will cause a slight change in the profile drag coefficient C_{D_o}.

Due to the increased down loading on the elevator and horizontal tail, the wing will have to develop more lift to maintain equilibrium conditions. This change in coefficient of lift C_L will change the induced drag and it must be incorporated in the incremental drag equation. The change in induced drag ΔD for a parabolic drag polar is

$$D_i = \frac{(L + \Delta L)^2 - L^2}{\pi A R e q_o S} = \frac{2L(\Delta L) + (\Delta L)^2}{\pi A R e q_o S} \cong \frac{2L\ \Delta L}{\pi A R e q_o S} \tag{9}$$

The lift increment ΔL can be expressed as

$$\Delta L = q_o S \Delta C_L = q_o S\ a_o \Delta\alpha \cong q_o S a_o \Delta\gamma \tag{10}$$

The lift L can be equated to the weight and drag by use of Figure (1).

$$L = W - T \sin\gamma = W - D \tan\gamma \tag{11}$$

Substituting equations (10) and (11) into (9) and letting $\tan\gamma = \gamma$ gives

$$\Delta D_i = \frac{2\ a_o \Delta\gamma\ (W - D\gamma)}{\pi A R e} \tag{12}$$

The incremental drag ΔD now consists of the drag chute ΔD_D and the change in induced drag ΔD_i. Substituting these expressions for ΔD in equation (7) and neglecting the product of γ and $\Delta\gamma$ yields

$$D = \frac{2a_o \Delta\gamma W + \pi A R e\ \Delta D_D}{\pi A R e[(1 + \frac{\Delta SHP}{SHP})E_p - 1]} \tag{13}$$

The incremental drag equation has now become much more complex. The values of a_o and e are unknown. They would have to be computed by theoretical or empirical means and would introduce errors in an equation which has already potential sources of error introduced by several simplifying assump-

tions.

The drag chute must be attached in such a way that the changes in induced and profile drag are very small. The chute used in the experimental program is attached to the tail so that it is closely aligned with the c.g. of the aircraft, and the drag of the chute is kept small (less than 10% of the total drag) to minimize pitching moments and the associated changes in C_{D_i} and C_{D_o}. This infers that the changes in profile and induced drag can be neglected and equations (7) and (8) can be evaluated for the aircraft drag.

The test aircraft was a Navy Model T-34B (Fig. 3), manufactured by Beech Aircraft Corporation. The T-34B is an all-metal, low wing, two-place tandem trainer. It has a constant-speed propeller, retractable landing gear, and is powered by a Continental Model O-470-4, a six-cylinder, horizintally opposed, air-cooled engine. The aircraft was chosen because its size, performance, and flight characteristics are typical of modern single engine general aviation aircraft.

The aircraft's standard propeller had been previously removed and replaced with a Hartzell Model FC8468 R. This is a two-bladed, full feathering propeller with an activity factor of ninety. It had been installed for use in gliding flight tests and was left on the aircraft for the incremental drag project.

The propeller torque was one of the most important parameters measured. For this, an aircraft propeller torquemeter, model 1308 manufactured by Lebow Associates, Inc., was mounted between the propeller and the aircraft engine (Fig. 4). The torquemeter consists basically of two parts, a fixed outer case and a rotating inner shaft. The shaft is mounted between the engine

and the propeller and becomes an extension of the engine propeller shaft. The outer case of the torquemeter is held fixed by retaining straps to prevent it from turning. As torque is applied to the propeller through the torquemeter, strain gauges mounted on the torquemeter shaft measure the deformation of the shaft due to the transmitted power. This deformation produces a voltage change in the strain gauges proportional to the propeller torque. The voltage is then transmitted via slip rings to the outer case and then to a transducer indicator.

The torquemeter output in this case was measured by a digital transducer indicator model 7510, manufactured by Lebow Associates, Inc. The instrument was powered by a 115 VAC, 60 Hz voltage and was calibrated to display the output in foot-pounds. Thus, the engine torque was recorded directly by the observer in the rear seat.

A tachometer is normally used to measure the propeller rpm. However, to improve the accuracy of measurement, a counter was used to measure the propeller speed directly. A magnetic pickup was mounted on the aircraft magneto. As the magneto made one revolution, a pulse signal was generated and sent to a Hewlitt-Packard model 5301 counter. The instrument counted the pulses over a ten second time base and displayed the result in digital form. Since the magnetos made three revolutions for every two propeller revolutions, the counter displayed a value equal to one-fourth the propeller rpm to the observer. By directly counting the propeller rpm, as opposed to using an analog output, an accuracy of ± 4 rpm was achieved.

The drag chute was the simplest, yet one of the most important pieces of equipment on the test aircraft since it generated the incremental drag for the flight test. The drag chute (Fig. 5) configuration was similar to that

of a wind sock. Its leading edge was made of 3/16 inch aluminum rod bent to form either an eight or ten inch diameter circle. Light cotton material was then sewn over the hoop to form a windsock approximately 14 inches long. The trailing end of the chute was reefed with a drawstring to form a 4 inch diameter circle at the tail to control the drag of the chute and make it stable in all flight configurations. The chute was attached to the aircraft with a thirty-nine foot long 3/32 inch nylon cord. The nylon cord was used because of its light weight, durability and strength.

Once the drag chute was deployed, the value of the incremental drag it created had to be accurately measured. To do this, a Gould, Inc. load cell Model UL 4-50 was used. To accurately measure the drag, the load cell had to be securely attached to the aircraft yet free to align itself with the pull of the drag chute. The attachment device also had to have a capability to allow jettisoning of the drag chute prior to landing. To accomplish this, the load cell was configured as shown in Figure 6. The regular tail cone was removed from the aircraft and a .004 inch bracket made of 4130 steel was riveted across the opening in the tail. This would ultimately secure the load cell assembly to the aircraft. A holder was then made for the load cell which consisted of a 2024 aluminum tube 3 1/4 inches long with an inside diameter of 1 1/8 inch. The load cell fitted inside one end and was held in place with four retaining bolts. The other end of the tube was closed and had a universal joint attached to it. The universal joint was bolted to the bracket across the tail, thus insuring the load cell was attached to the aircraft, but aligned with the drag chute. To release the drag chute a 7 1/2 inch long, 3/16 inch diameter steel rod was constructed with a tow release hook on one end. The hook release was controlled by a cable running

to the pilots' compartment. The other end of the rod was threaded and screwed into the load cell. To prevent the load cell assembly from striking the side of the aircraft during chute release, a cushioning ring was fitted around the assembly. This consisted of foam rubber 3 1/2 inches in diameter and 1 inch thick. The rubber fitted around the load cell assembly and was held in place by a 3 1/2 inch diameter ring made of .0040 thick 4130 steel. The steel ring was then supported and bolted to the tail section of the aircraft. This entire assembly allowed the load cell to align with the drag chute, but prevented it from making large and abrupt movements that might damage the load cell. The load cell flexure strain gauges were powered by a five volt DC power supply.

Since the output voltage of the load cell was very low (approximately 5 mV. at full scale) the output was amplified by a factor of 40 and then displayed on two Datel digital panel meters. One meter was in the back seat for use by the observer. Since the drag chute was directly behind the aircraft in flight, it was very difficult to observe during the flight test. The meter enabled the observer to tell if the drag chute was attached and to see if it was stable during the flight. The other meter was mounted on a photopanel which provided a time history of the chute during the flight test and gave a permanent record for the data reduction procedure.

The parameters measured by the air data system were the indicated airspeed, indicated pressure altitude, outside air temperature, and relative angle of attack. These were used to determine true airspeed, pressure altitude, air density, and change in angle of attack.

The boom and flying head (Fig. 7) was used to measure the static pressure, total pressure, and the angle of attack. By placing the sensor head

five feet in front of the leading edge of the wing, it was possible to minimize errors in the static pressure field and the angle of attack.

The outside air temperature probe was mounted under the left wing of the aircraft. (Fig. 8) The sensing element of the probe was a Model 35J3 thermistor made by Omega Engineering, Inc. The element was enclosed in a perforated radiation shield to minimize sensing error. The thermistor measures temperature by incorporating a temperature-sensitive resister. As the temperature changes, the output voltage of the thermistor changes. Once calibrated, the thermistor can provide very accurate temperature data.

The angle of attack relative to the boom was measured in a similar fashion. A potentiometer was installed in the boom and connected to the flying head so that as the head moved up or down the resistance of the potentiometer was changed. A five-volt input was applied and the output displayed on a Datel digital panel meter mounted on the observer's panel.

The photopanel (Fig. 9) mounted in the aircraft fuselage was the primary data source where chute drag, outside air temperature, airspeed, and altitude were all recorded. The chute drag and outside air temperature voltages were put through a two-channel multiplexer and displayed on the Datel digital meter to alternately display the chute drag and the OAT. A small light was mounted in the upper left hand corner to illuminate whenever chute drag was displayed. This provided a discriminator for the two outputs. The total and static pressure tubes from the left wing probe were connected to the airspeed indicator and altimeter mounted on the photopanel. A clock was mounted on the panel to display the test time. A binary display light system was mounted on the bottom of the photopanel which consisted of four lights connected to a digital decade counter that was controlled by the observer. At each succeeding test point the counter was advanced once, thus changing the light sequence. By utilizing the lights as binary numbers, up to 15 points

in sequence could be differentiated on the photopanel. At any point the observer could reset the lights and begin a new sequence. The panel was illuminated by six 12 watt bulbs and photographed with a 16mm movie camera using Kodak Tri-X Reversal (ASA 160) film at a rate of 1 frame per second. The camera was controlled by an on-off switch located in the pilot's compartment.

A schematic of the electrically powered instruments and the associated power system is shown in Figure 10. All AC power was provided by an advanced design inverter powered by the 24 volt aircraft battery. The 115 VAC, 60 Hz output was wired to a four-plug junction box. This became the central source for all AC instruments shown and the five volt DC power supply for the angle of attack probe and the Datel digital panel meters. The photopanel camera, lights, and OAT probe were powered by rechargeable five volt and ten volt batteries. These were recharged frequently to insure proper operating voltage and power output.

The data acquisition system output was thus displayed in two places. The observer recorded engine torque, rpm, and angle of attack. He could also observe the drag chute output. Figure 11 is a photo of the observer's instrumentation. The drag chute output and air data system were recorded on the photopanel. This insured that steady-state flight conditions had been achieved and provided a permanent record of the flight.

All instruments except the airspeed indicator and altimeter were calibrated while on the aircraft and using the aircraft power system.

The altimeter and airspeed indicator were both calibrated at the MSU Department of Aerophysics and Aerospace instrument laboratory. The altimeter Kollsman window was set to 29.92" hg. The static pressure line of the

altimeter was connected through a "T" fitting to a vacuum source and a mercury barometer (Fig. 12). By varying the vacuum on the altimeter static line by use of a valve, the indicated altitude was changed from -60 to +16, 400 and back to -50 feet in increments of 500-2000 feet. The mercury barometer, corrected for non-standard temperature, gave the pressure on the altimeter at each test point. This pressure was then converted to a pressure altitude. The difference between the true pressure altitude and the indicated altitude was the instrument error. This was plotted versus indicated altitude to form an altimeter calibration curve (Fig. 13).

A similar procedure was used for the airspeed indicator. The total pressure line of the airspeed indicator was connected through a "T" to a high pressure source. A Betz water manometer was used to measure the pressure going to the airspeed indicator. The airspeed was varied from 50 knots to 150 knots and back to 50 by varying the input pressure. The pressure indicated at each point by the manometer was then converted to an equivalent airspeed at sea level. The difference between the equivalent airspeed and the indicated airspeed was the instrument error. This was plotted versus indicated airspeed to form an airspeed indicator calibration curve (Fig. 14).

The position error for the airspeed indicator induced by local variations in pressure at the airplane static source was found by flying a surveyed ground course in both directions at a constant indicated airspeed and altitude. The indicated airspeed for the course was corrected for instrument error and converted to a true airspeed. The difference between the true airspeed and the average ground speed for both runs was the instrument position error. This is plotted versus the indicated airspeed corrected for instrument error in Figure 15.

The torquemeter and transducer indicator were factory calibrated by the manufacturer, Lebow, Inc. After the instruments were installed on the aircraft, the propeller torquemeter was checked for small torque values by adding weights at the propeller tip to create a torque. This procedure allowed calibration of the system to torque up to 25 ft-lb which is only about 8% of the range of interest. Tests of higher torque values was not possible since there was no way to keep the engine from rotating.

The transducer indicator had a precision resistor installed on it for calibration purposes. By depressing the calibration span switch, the 120 KΩ resister simulated a torque of 500.5 ft-lbs. The indicator could then be zeroed and calibrated for that load.

The drag chute load cell was calibrated after it was installed on the aircraft by a dead weight method. Weights were connected to the load cell by a cable and hung over a low friction pulley. The weights were varied from zero to 40 lbs. and back to zero in 10 lb. increments. This process was repeated to check for linearity and hysteresis of the load cell output. This calibration is shown in Figure 16.

The angle of attack sensor was calibrated by mounting a protractor on the test boom in such a way that the probe angular position could be measured relative to the beam. The probe was then varied between -8° and +18° in increments of one degree. All angles were measured with respect to the center line of the boom. The graph of angle of attack versus voltage output is shown in Figure 17.

In addition, the outside air temperature (OAT) probe was calibrated by simulating the temperature with a precision potentiometer. Since the resistance of the thermistor is known as a function of temperature, the OAT system

was calibrated by varying the resistance of the potentiometer and recording the output voltage. The resistances were then converted to temperatures and a plot of temperature versus output voltage was made (Fig. 18).

Since the tachometer counter is not an analog instrument, but a digital counter, no calibration was necessary for the propeller rpm.

The flight test procedure was designed to generate aircraft power required performance curves for the clean airplane and for the airplane plus drogue combination. All data was reduced to standard sea level conditions. These are arranged so that the power required for level flight (with and without the drogue) can be used with the measured drag increment caused by the drogue to compute the airplane drag.

All test flights were conducted in early morning calm air to minimize convective turbulence. The test pressure altitude was selected to be six thousand feet, but had to be varied somewhat to avoid wind-shear turbulence. It is absolutely essential to have turbulent free air in order to insure good flight path control.

The flight test procedure is simple and a routine part of aircraft development. Manufacturers typically generate power required curves for use in pilot handbooks and performance specifications. The use of an incremental drag device is of course different and requires one additional flight test sequence to yield aircraft drag and propeller efficiency values. Following level-off at the selected pressure altitude, the aircraft was stabilized in straight and level flight at an indicated airspeed of approximately 60 knots and a propeller speed of 2000 rpm. This propeller speed was selected and held fixed for all test points in order to maximize propeller advance ratio and minimize the efficiency changes associated with changes in power. The

photopanel camera was then turned on to record airspeed, altitude, time, OAT, and chute drag if installed. At the same time the engine torque, propeller rpm, angle of attack, and chute drag were recorded by the observer in the aircraft. After the data was recorded, the camera was turned off and the airspeed was increased 3 - 10 knots by changing the engine manifold pressure approximately 0.5 inches. After the aircraft was stabilized at the new airspeed, the data recording process was then repeated.

The airspeeds and power settings were continually increased until maximum power and speed were obtained. The flight test procedure was then reversed and the airspeed reduced in increements of 3 - 10 knots by reducing the manifold pressure in 0.5 inch increments. This was continued until the point of minimum power was reached. The flight test was then terminated and the aircraft returned for landing.

The drag chute, if installed, was released just prior to touchdown to prevent dragging the chute on the runway. After landing the photopanel camera was turned on to record the landing time and the load cell zero. The torquemeter zero and the angle of attack reading at full scale deflection were also recorded by the observer to check for zero shifts. After the aircraft was refueled, the fuel load at landing was computed and recorded on the data sheet. The computed fuel consumption was used to calculate the weight during the flight.

The film used in the photopanel was then removed from the camera and processed for use in the data reduction procedure.

The data reduction process is a systematic method of converting raw flight test data into a standardized format that can be utilized by the flight test engineer. The raw data in this case consisted of the indicated airspeed,

indicated pressure altitude, the outside air temperature, engine torque, propeller RPM/4, the chute drag, and aircraft fuel weight. The airspeed, altitude, OAT and chute drag (in mV) were found by time averaging the values displayed on the photo panel at each test point. The torque and RPM/4 were obtained from the engineer's data sheet. The fuel on board was estimated at each test point by calculating the fuel consumption rate in gallons per minute during the flight. By assuming a linear reduction in fuel and knowing the takeoff and test point times, the fuel weight at the test point could be calculated.

The raw data, along with the passenger weight and the load cell zero, were then read into a program on the UNIVAC 1106 computer. This program calculated and printed the values of generalized velocity VIW, generalized power PIW, the equivalent airspeed V_e, the dynamic pressure q, and the chute drag ΔD for each test point. The standard weight used for the generalized power and velocity was 3000 pounds.

A plot of PIW versus VIW for each of the three test configurations was then drawn (Fig. 19, 20, 21) to obtain a power required curve for a standard weight airplane at standard sea level conditions. Since there was some scatter of the test points, a curve of the form

$$PIW = A(VIW)^3 + B(VIW)^{-1}$$

was fitted through the points by using a least-squares routine to find the value of A and B for each graph. By using this equation, the power required with and without the drag chute could be computed directly.

A similar procedure was followed for the chute drag. A plot of drag versus dynamic pressure was made for the small and large chutes (Fig. 22).

A line of the form

$$\Delta D = Aq + B$$

was fitted through the points by using a least-squares routine to calculate the values of A and B for the small and large drag chutes. The chute drag could then be found at each velocity by calculating the dynamic pressure q.

Once expressions for the power required and chute drag were found, it was possible to calculate the aircraft drag using the incremental drag equations.

The first equation assumes constant propeller efficiency. However, the second drag equation requires calculation of E_p, the propeller efficiency ratio. Two different methods were used to find values of E_p.

The first involved using a computer program developed by the Hamilton Standard Propeller Company. The program used a modified Goldstein theory to calculate the thrust of a free propeller for specified flight conditions. The program was modified to print out propeller efficiency directly. By putting in the power and velocity with and without the drag chute, the propeller efficiencies could be found and the resulting E_p calculated.

The second method used a chart (Fig. 23) developed from research conducted by NACA during World War II. By knowing the advance ratio J and coefficient of power C_p, the value of the coefficient of thrust C_T can be found. The propeller efficiency η_p is calculated as

$$\eta_p = \frac{C_T}{C_p} J$$

By finding the values of C_T and C_p with and without the drag chute, the values of η_p and E_p could be found.

Aircraft drag data is conventionally presented in drag polar form, which is

a plot of the coefficient of drag C_D versus the lift coefficient squared C_L^2. Since most aircraft exhibit a parabolic drag polar of the form

$$C_D = C_{DO} + KC_L^2$$

in the low Mach regime, the graph of C_D versus C_L^2 should give a straight line with a slope of K and a zero intercept equal to C_{DO}.

After the drag polar was constructed, a linear regression of C_D upon C_L^2 was used to find the values of C_{DO} and K and to fair a line through the points of the graph.

The basic incremental drag expression

$$D = \frac{\Delta D \times P_1}{P_2 - P_1}$$

is the simplest and most practical of the three equations evaluated. The propeller efficiency for this case is assumed to be constant for the power range P_1 to P_2 and thus E_p, the propulsive efficiency ratio, is equal to one.

Flight test data for the small drag chute is shown in Table 1 and the associated drag polar in Figure 24. These test points were evaluated between 90 and 110 knots. This is within the normal operating speed of the aircraft and minimized the scatter found in the lower portions of the PIW - VIW curve. The results in Table 1 show the drag decreasing to a minimum value at approximately 100 knots and then increasing as the speed decreases to near stall. The propulsive efficiency η_p is fairly high but is decreasing with increasing velocity. The drag polar shows a straight line with $C_{DO} = .0208$ and a value of $K = .0876$. The following analysis and commentary addresses the probable validity of these results.

The minimum drag velocity can be calculated if the aircraft has a parabolic drag polar. This seems to be very reasonable, since the C_D vs C_L^2 curve is nearly linear. Thus, the expression for minimum drag velocity is

$$V_R = \sqrt{\frac{2}{\rho}\frac{W}{S}} \qquad \sqrt[4]{\frac{K}{C_{DO}}}$$

where V_R is the minimum drag velocity, ρ is the air density, W the aircraft weight, S the wing area, C_{DO} the profile drag coefficient, and K is the slope of the $C_D - C_L^2$ curve and is equal to $(\pi AR e)^{-1}$. Using the value of C_{DO}

and K obtained from the drag polar and the standard air density and aircraft weight gives

$$V_R = \sqrt{\frac{2 \times 3000}{.0023769 \times 177.6}} \quad \sqrt[4]{\frac{.0876}{.0208}} = 170.8 \text{ ft/sec} = 101 \text{ knots}$$

Thus, the minimum drag velocity obtained from the incremental drag equation and the small chute flight test data agrees almost exactly with the predicted value.

The drag polar values of C_{DO} and K can be compared with gliding flight tests conducted at the MSU Raspet Flight Research Laboratory. Those results showed values of $C_{DO} = 0.0235$ and $K = .0604$. It is likely that the value of C_{DO} measured in level flight will be higher than that measured in gliding flight due to the increased drag of the propeller and slipstream effects. However, the augmentor-type cooling system used on the test aircraft is an additional complication. The augmentor tubes produce a small amount of thrust when the aircraft is in powered flight. They produce no thrust in power-off gliding flight. This added thrust would show up as reduced aircraft drag in flight and thus lower the C_{DO}.

It is possible, though, to estimate the thrust produced by the augmentor tubes. Calculations supplied by Mr. Frank Monts, Cessna Aircraft Company, show a 1.6 horsepower increase at 90 miles per hour and full power on a standard day at sea level. This equates to an additional 6.7 lbs. of thrust. This amount of thrust would reduce the measured C_{DO} by only .0018. It is likely that the working propeller and the additional drag due to the slipstream would be greater than this value. Thus the predicted C_{DO} from the incremental drag equation using the small chute appears to be too low.

Since $K = (\pi ARe)^{-1}$, the differences in K are due to the changes in the wing efficiency factor e. It is possible to estimate the value of e for a free wing. Using a value of the taper ratio $\lambda = 0.5$ and the

aspect ratio AR = 6.06 gives a value of e = 0.98. This will be changed, however, by the effect of the fuselage and the propeller slipstream. It is likely that the value of e = 0.87 in gliding flight is correct. However, due to the interaction of the fuselage and wing with the propeller slipstream, it is impossible to judge whether e will increase or decrease with the addition of power. Whether the computed value of K is "correct" is impossible to say.

A small chute was initially selected to minimize the propeller efficiency changes so that E_p could be set equal to one. However, the associated power changes were so low that the drag equation became limited by the resolution of the instrumentation. Since the denominator of the equation consists of a small difference of power (4.7 to 8.4 HP), a one percent error in P_1 and P_2 can result in a 12 - 17% error in aircraft drag. One solution to this problem is to go to a larger drag chute to increase the value of $P_2 - P_1$.

The incremental drag data using the large drag chute is shown in Table 2 and Figure 24. The velocities are again limited between 90 and 110 knots.

The total indicated aircraft drag obtained with the large chute was less than with the small chute. The values of C_{DO} and K, however, were much closer to that of the gliding flight data. It is possible again to calculate and compare the minimum drag velocities. Using the calculated values of the C_{DO} and K gives

$$V_R = \sqrt{\frac{2 \times 3000}{.0023769 \times 177.6}} \qquad \sqrt[4]{\frac{.0528}{.0243}} = 144.7 \text{ ft/sec} = 85.710$$

However, the aircraft flight test drag did not exhibit a minimum point at 85.7 knots or at any other velocity. Extrapolating the incremental drag equation to lower velocities simply resulted in the aircraft drag getting smaller.

Extrapolation of curves, however, is a dangerous business. The calculations were originally limited between 90 and 110 knots to exclude regions of unacceptable scatter. Examination of the PIW - VIW curve with the large drag chute installed (Fig. 21) shows a large amount of scatter below 90 knots which is not unusual for this flight region. This, however, makes it impossible to draw any conclusions from the behavior of the drag data outside the range of good curve fit. It is possible to compare the calculated minimum drag speed with the minimum drag speed listed in the aircraft operating manual. The manual lists 90 knots as best glide or minimum drag speed. This compares very favorably with the predicted value of 87 knots from the computed C_{DO} and K.

The computed value of C_{DO} = 0.0243 was slightly higher than that derived from the gliding flight data. As stated previously, that result would be expected. Computing the value of the wing efficiency factor yields a value of e = .995. This is greater than the gliding flight value of e = 0.87. Again it is impossible to predict the effect of the fuselage and wing interaction with the slipstream. It is possible, however, that the increased velocity of the slipstream produces a rise in lift at the wing-body and a corresponding rise in e. More flight test will be needed to confirm the calculated values of e and K.

Since different values of C_{DO} and K were found with the small and large drag chutes, an attempt was made to account for the possible change in propeller efficiency by calculating a value of E_p.

Two different methods of calculating E_p were tried. The first method used the computer program in NASA CR 2066 to calculate the propeller efficiencies and E_p. The results for both the small and large chutes are shown in Table 3, Table 4 and Figure 25. The results were actually worse when trying to correct for E_p. The computed drag polar is clearly non-linear and no attempt was made to fit a line through the points to

obtain C_{DO} and K.

Since the first method failed, a second attempt was made to correct for E_p by using the NACA Gray Charts. It was felt that these would be more accurate since they were based on wind tunnel tests of real propellers. The results of using the Gray Chart is shown in Tables 5 and 6 and Figure 26. These also show that the Gray Charts were unable to accurately provide a proper value of E_p. The computed drag polars of both the small and large drag chutes are characterized by scatter and non-linearity. No satisfactory value of E_p was found in either method.

The main problem in using a correction for E_p is that the incremental drag equation is ill-conditioned with respect to E_p. That is, a small change in E_p creates a large change in drag. As an example, the aircraft drag at 90 knots calculated by using the small chute and $E_p = 1$ was equal to 262.9 lbs. However, the same drag (V = 90 knots) using E = 1.010 was calculated to be 222.4 lbs. A one percent change in E_p produced a 15.4% in drag. This means that any error in E_p is greatly magnified in the resulting calculated drag. The required accuracy for E_p is not possible with the NASA computer program or the Gray Chart.

The propeller efficiency can be directly computed by using measured shaft horsepower and the corresponding aircraft drag values. These results are shown in Tables 1 and 2 for the large drag chutes.

The computed efficiency using the small chute started at a high value of .897 and decreased with increasing velocity. The large chute results, however, show the efficiency starting at a low value of .733 and increased with velocity. Again the problem arises as to what can these values be compared.

Both the computer program and the Gray Charts predict a propeller efficiency for an isolated propeller of .85 - .90 for the range of power and velocities used. However, they also predict that the efficiency

generally increases with velocity to around 105 knots and then slowly decreases.

The small chute efficiencies are closer to those predicted by the computer program and the wind tunnel tests. However, the predicted values do not take into account the losses in efficiency due to nacelle interference and increased fuselage drag. This could easily lower the propeller efficiencies to those values calculated by use of the large chute. It is likely that the large drag chute efficiencies are closer to the actual propeller efficiencies.

The third incremental drag equation was not evaluated due to the uncertainties in calculating E_p and the unknown values of a_o and e.

The incremental drag equation has been evaluated using two different drag chutes. The first set of calculations assumed a constant propeller efficiency at each test point. The second set of calculations used two methdos of calculating the relative change in propeller efficiency. Several conclusions can be drawn from the results.

The large chute data gave a more accurate value of profile and induced drag coefficients than the small chute. The incremental drag equation was able to measure the aircraft drag in level flight without assuming a value of propeller efficiency. The small chute data was not as accurate due to the lack of resolution in the small power changes required for the small drag chute.

It was possible to calculate the propulsive efficiency directly by using the aircraft drag computed from the basic incremental drag equation. This computed efficiency was the actual operating efficiency and included losses due to compressibility, interference, and slipstream effects.

Trying to correct for the small changes in propulsive efficiency was extremely difficult due to the nature of the incremental drag equation.

There is no current method of accurately predicting the propulsive efficiency or the relative change in propulsive efficiency. It appears that by using a constant-speed propeller the efficiency remained a constant and $E_p = 1.0$ as long as the chute is kept small.

Since these were the first results obtained from incremental drag, the conclusions must be regarded as tentative.

Additional flight tests will be conducted to verify the results found here. These will use various sizes of chutes to determine their effect on the computed drag and efficiency. The resolution of the instrumentation particularly the torquemeter, can be improved by in-flight zeroing of the instrument.

After the repeatability of the method is demonstrated, further tests will be conducted to determine the sensitivity of the method to small changes in aircraft drag. This could include flight with flaps partially extended or other drag producing items attached to the aircraft to check for changes in C_{DO}.

One other propeller will also be tested to check for efficiency. This will include testing at high tip speeds to check for compressibility and blade interference losses.

The basic incremental drag equation has the potential to provide profile and induced drag coefficients as accurately as those obtained from gliding flight. It can also be used to calculate the propeller efficiency directly, thus providing a unique way of measuring this unknown and very important parameter. Knowing the values of both drag and efficiency can then prove the design methodoly and performance prediction methods of all propeller-driven aircraft.

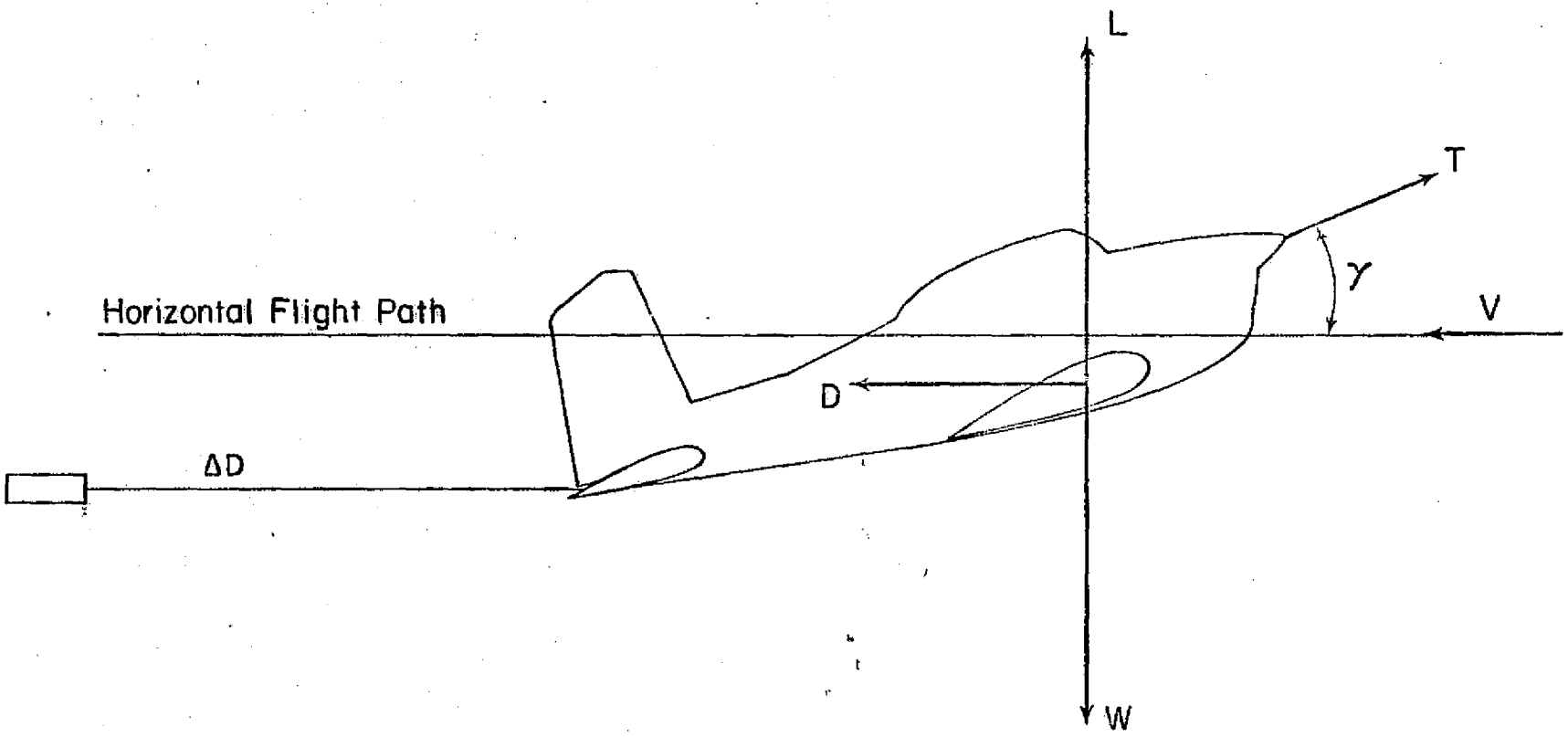

Figure 1. Aircraft Forces in Level Flight

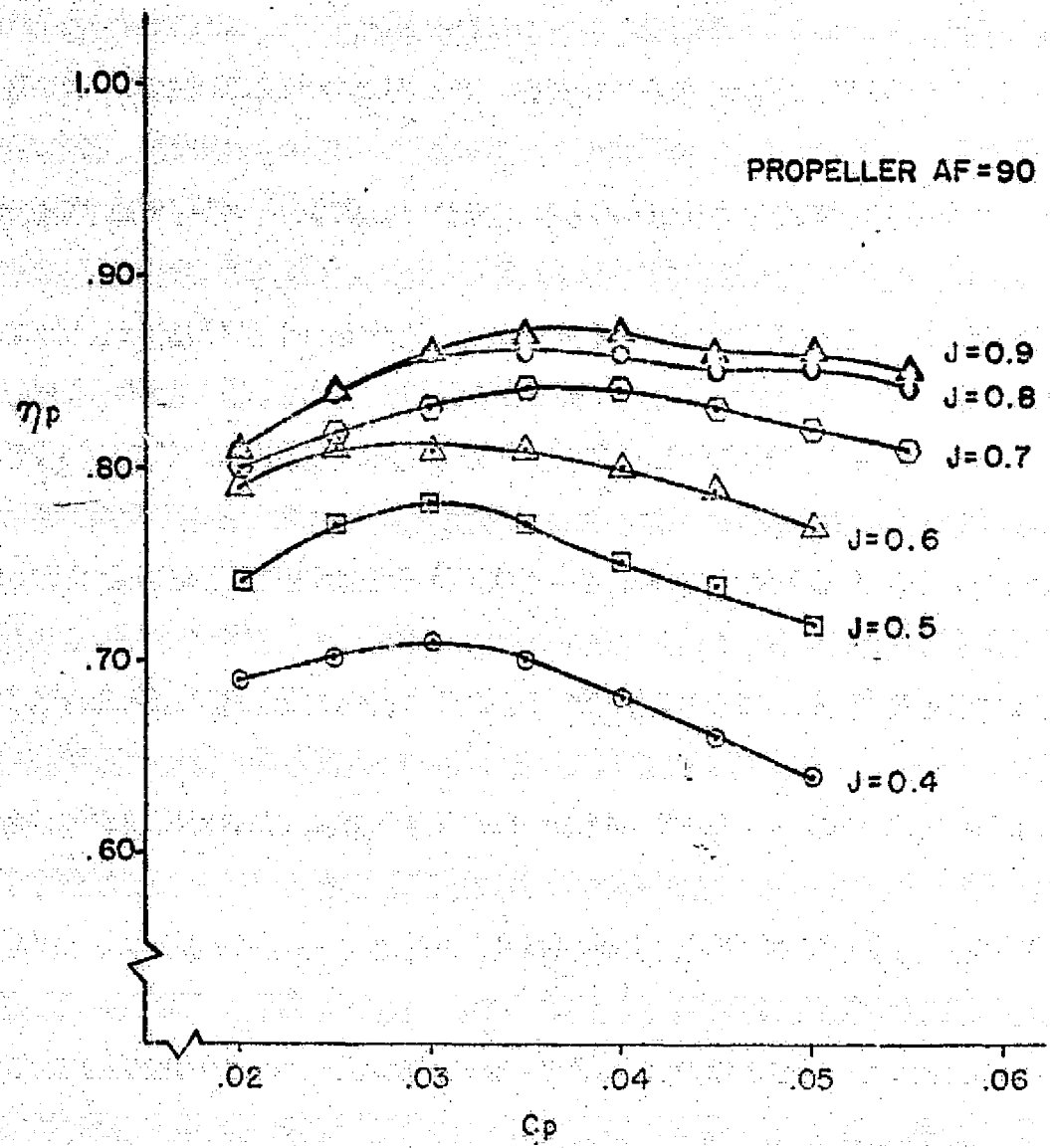

Figure 2. Propeller Efficiency versus Coefficient of Power

Figure 3. Flight Test Aircraft Beech T-34B

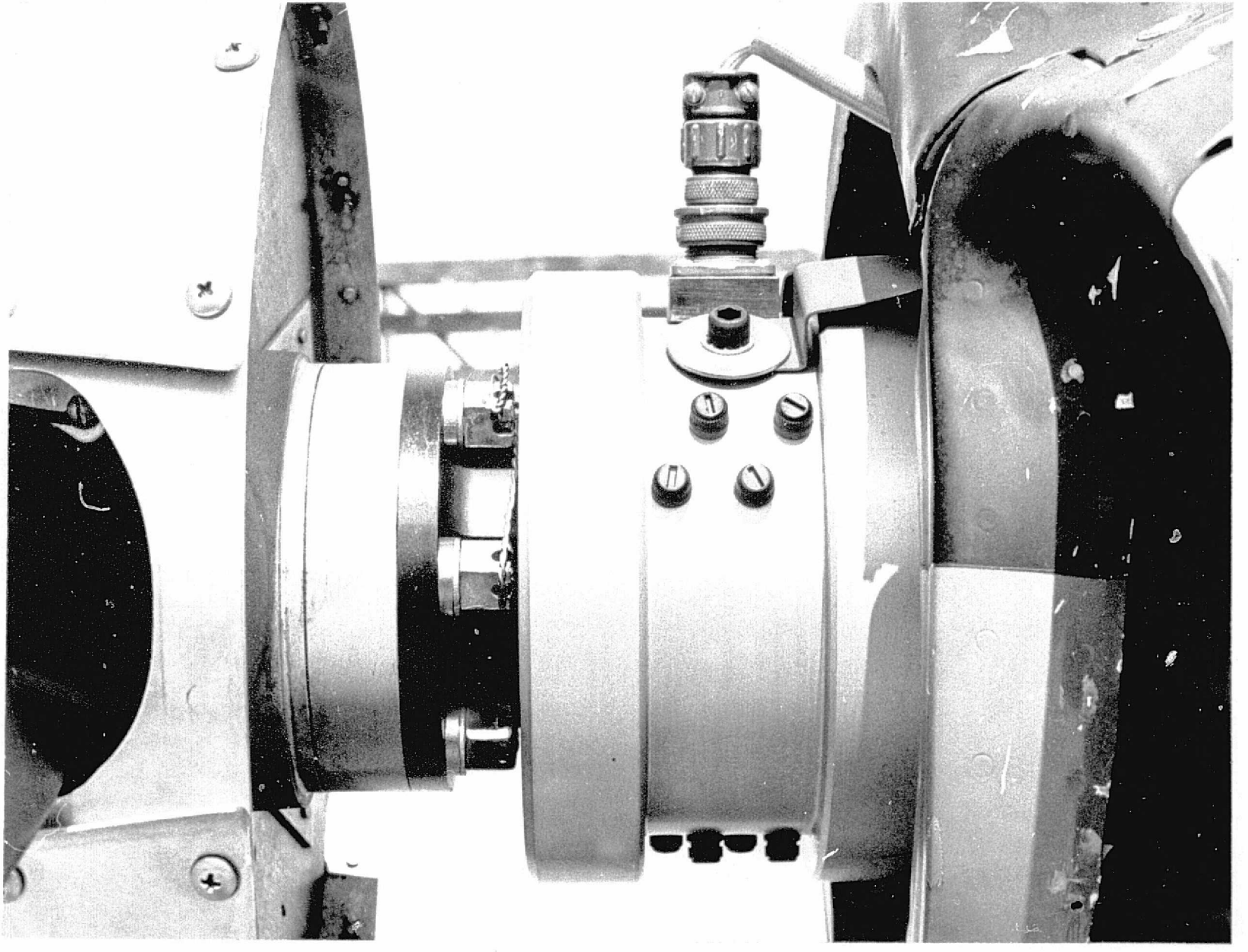

Figure 4. Torque Meter Installation

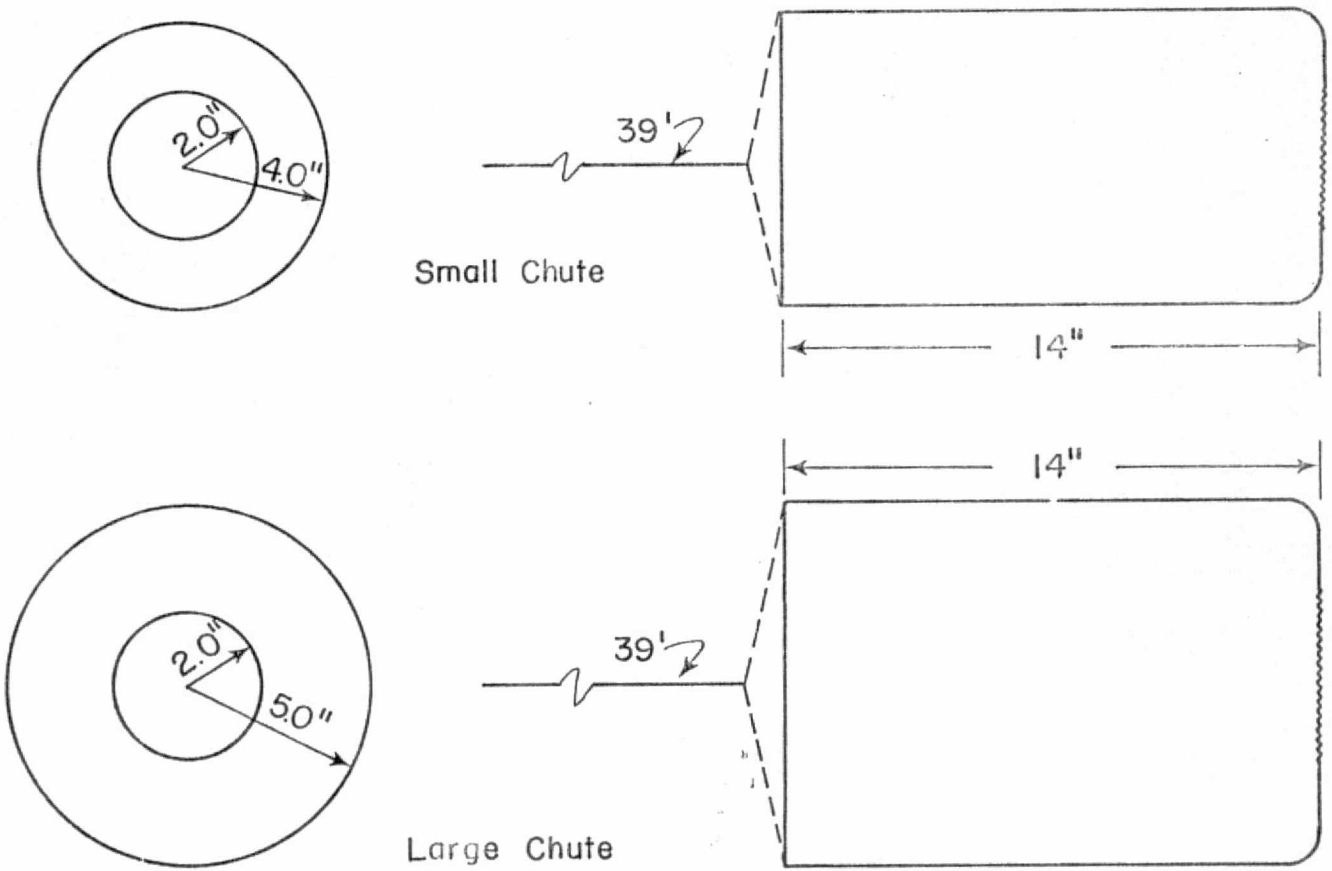

Figure 5. Schematic of Small and Large Drag Chutes

Figure 5a. Drogue in Flight

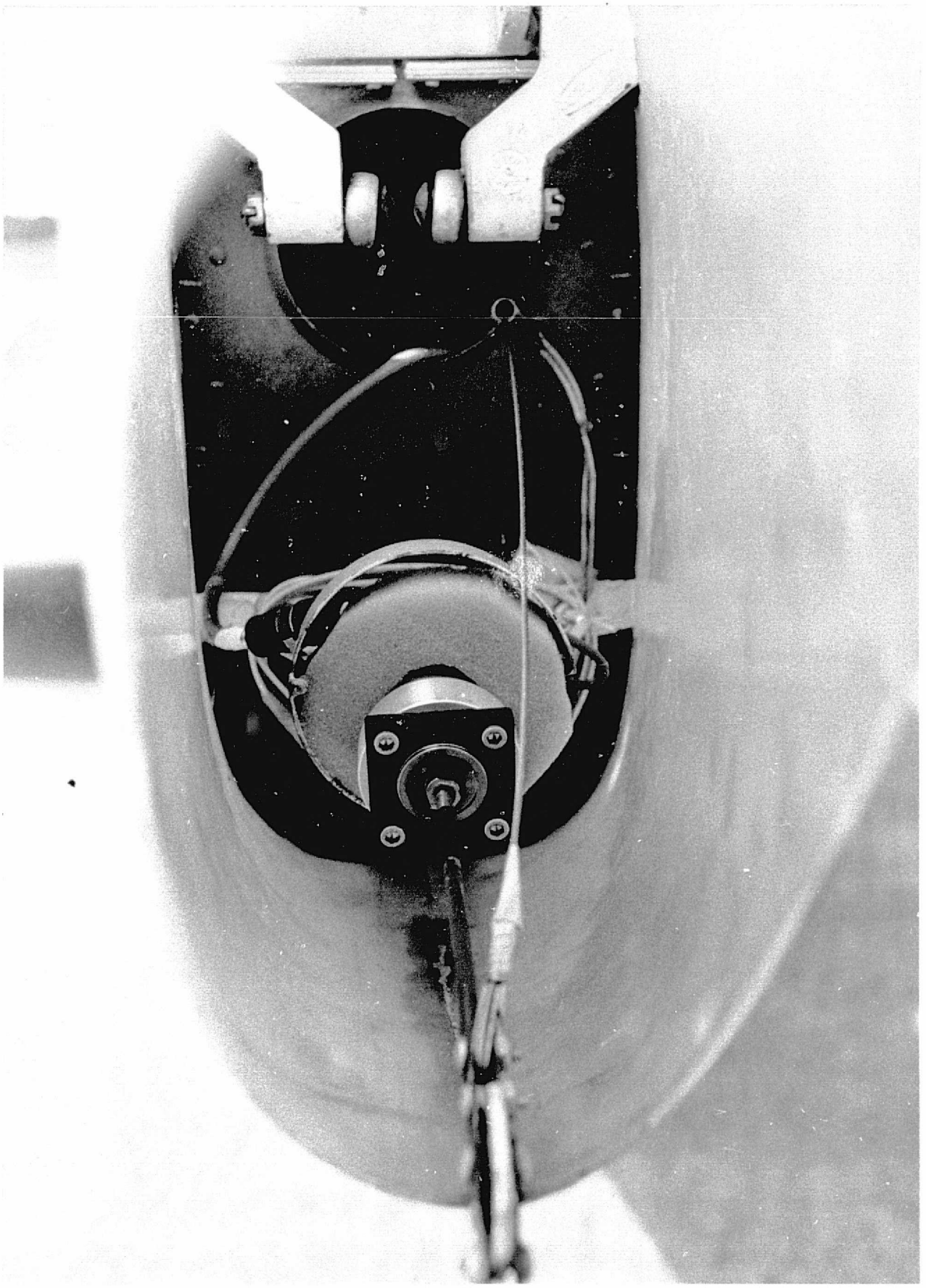

Figure 6. Load Cell Installation

Figure 7. Air Data Test Boom

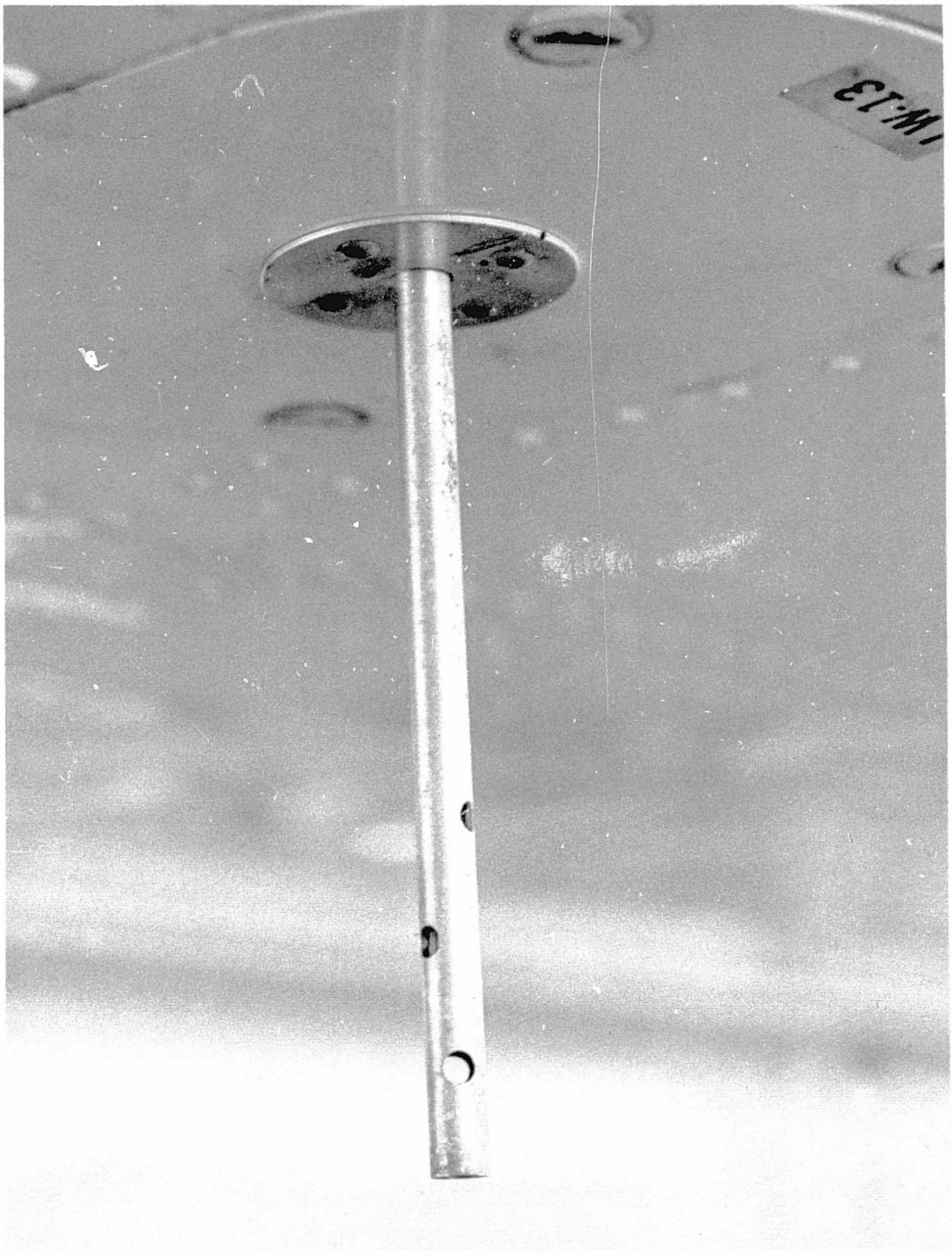

Figure 8. Outside Air Temperature Probe

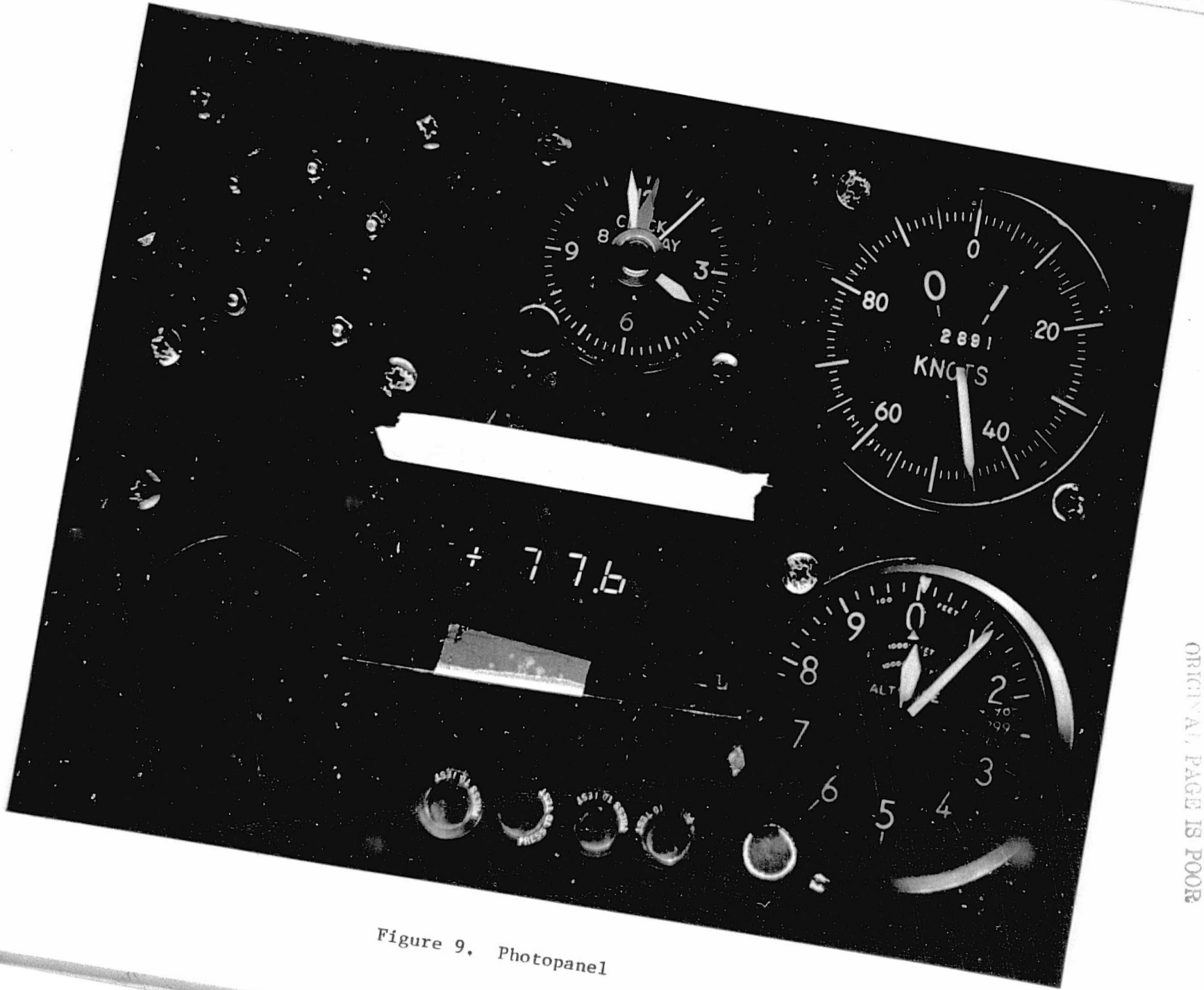

Figure 9. Photopanel

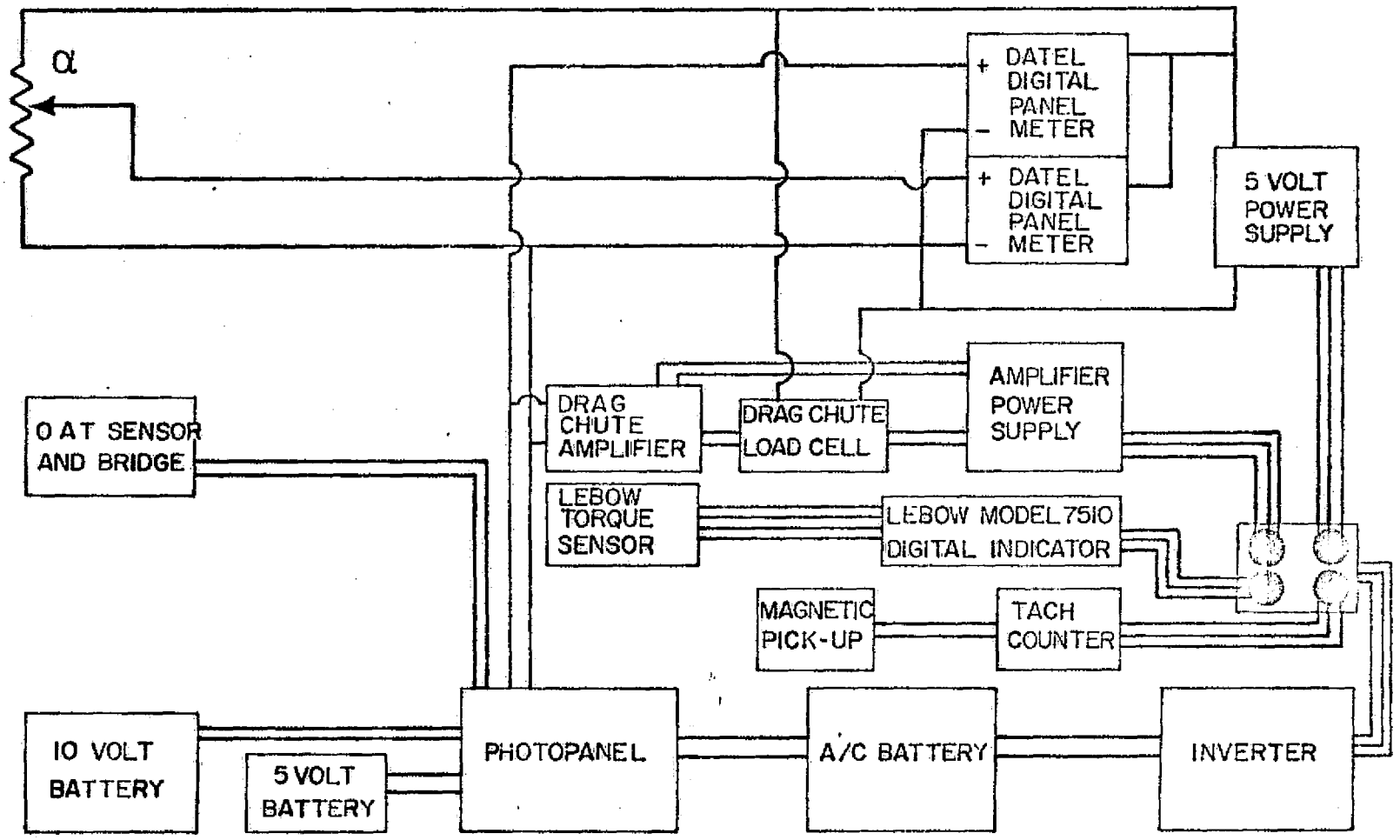

Figure 10. Schematic of Instrumentation Power System

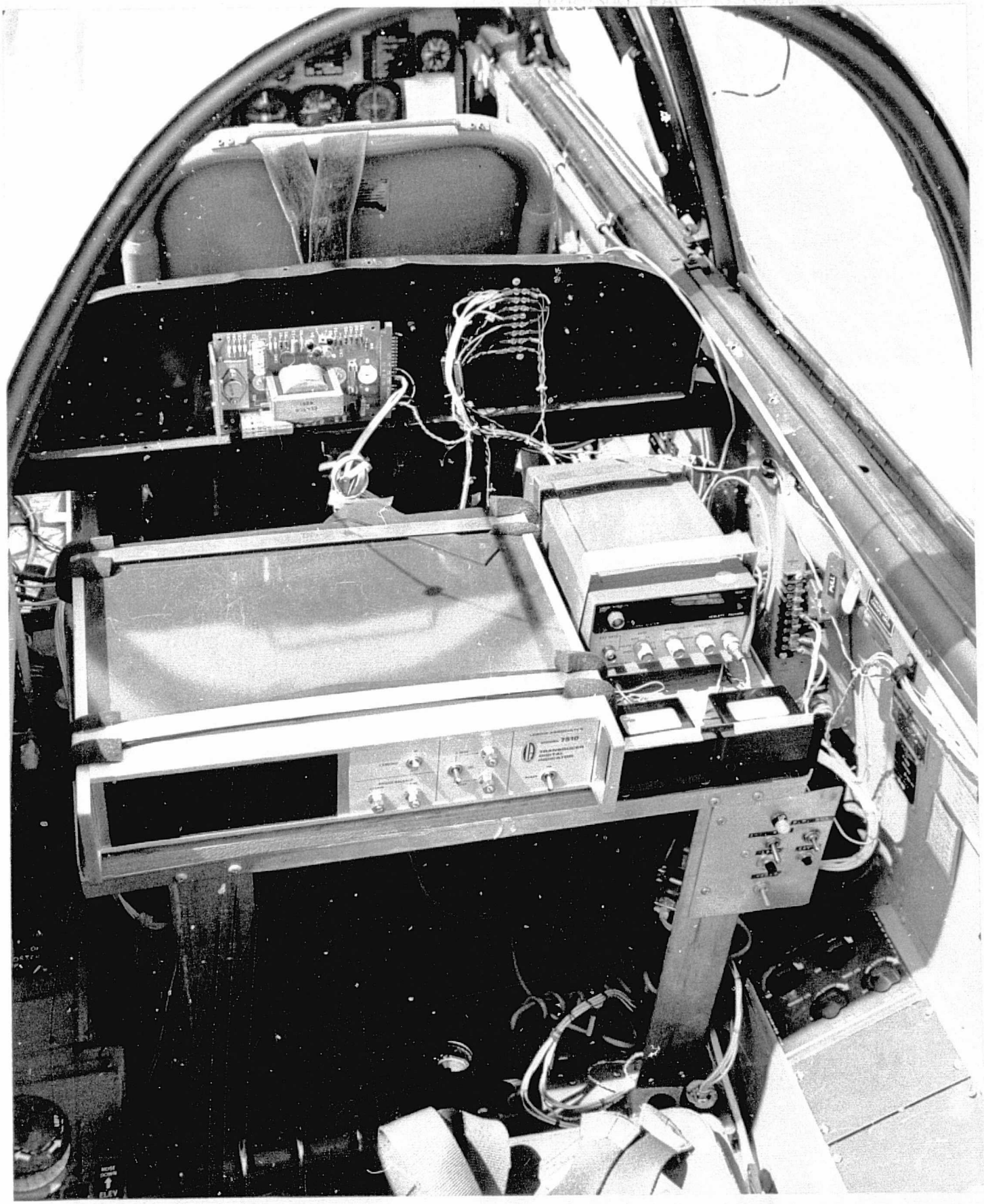

Figure 11. Flight Test Engineers Data Panel

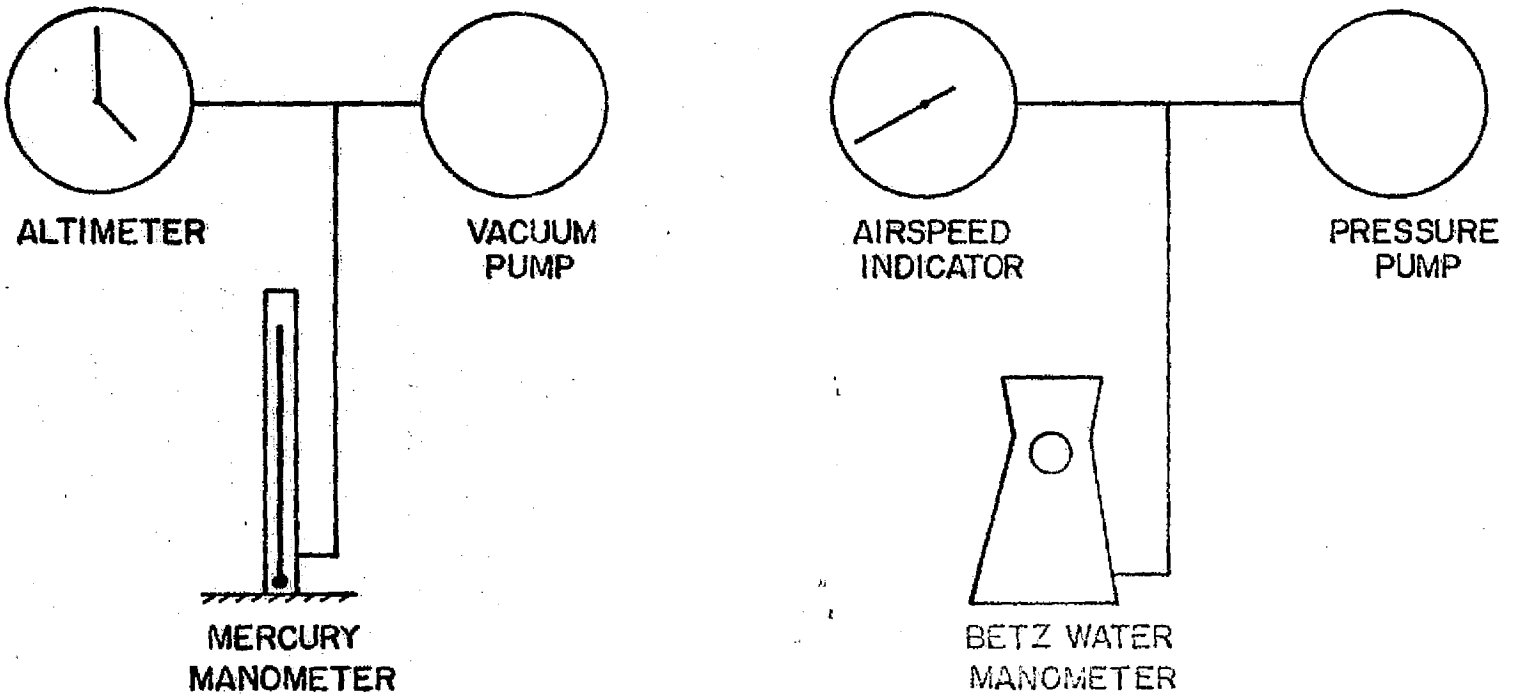

Figure 12. Schematic of Flight Instrument Calibration

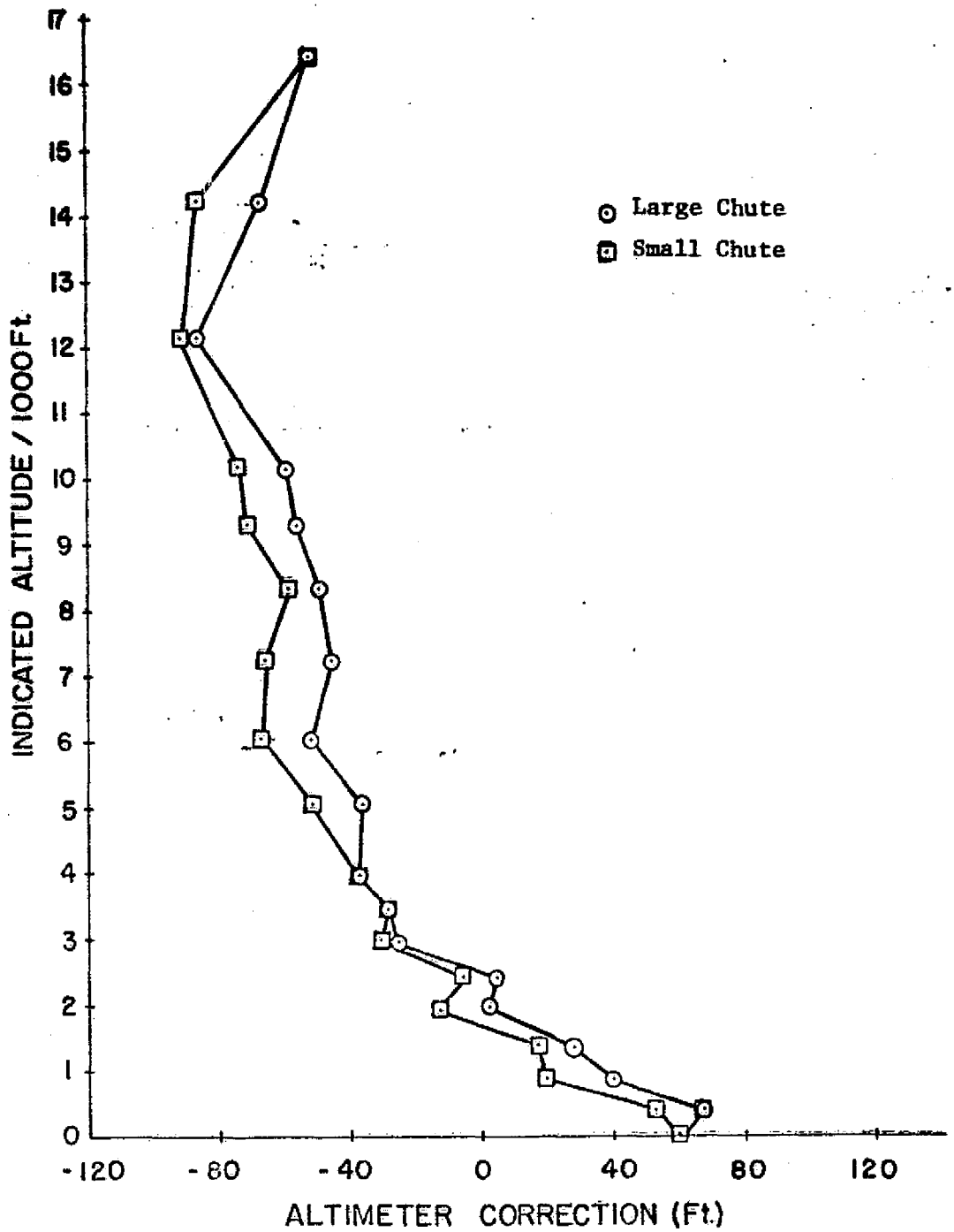

Figure 13. Altimeter Calibration Curve

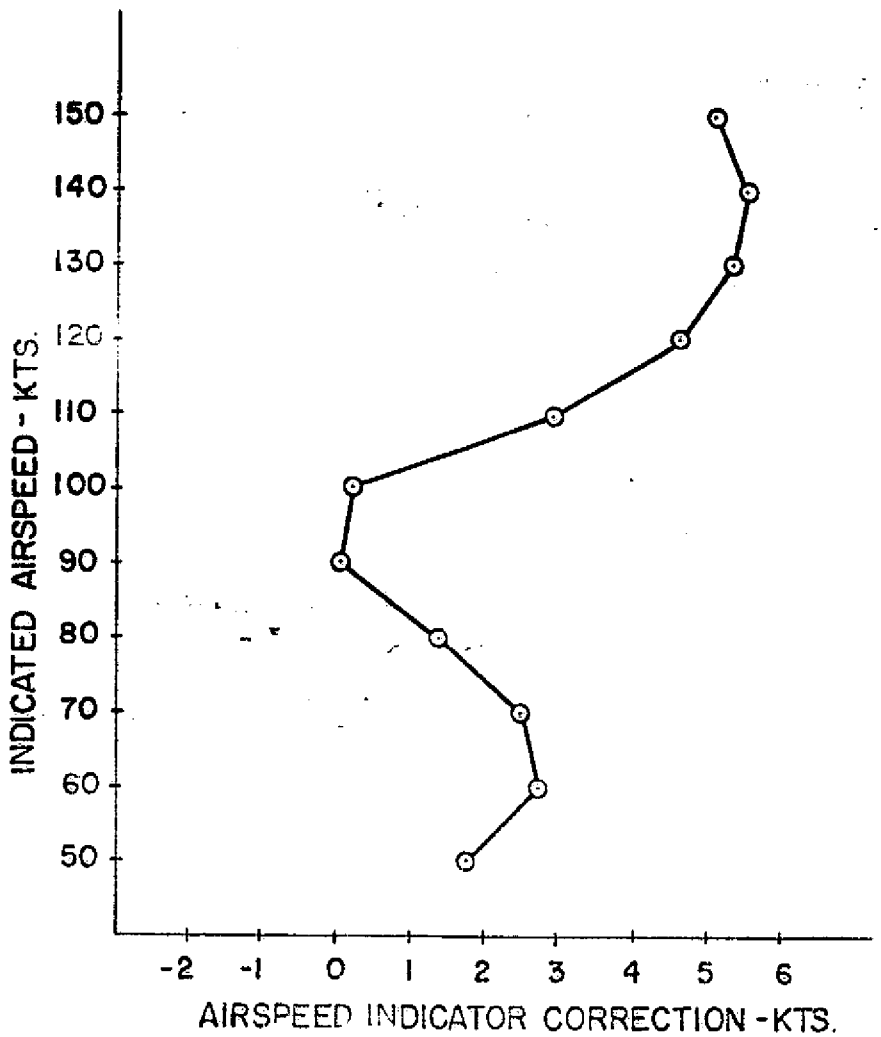

Figure 14. Airspeed Indicator Calibration Curve

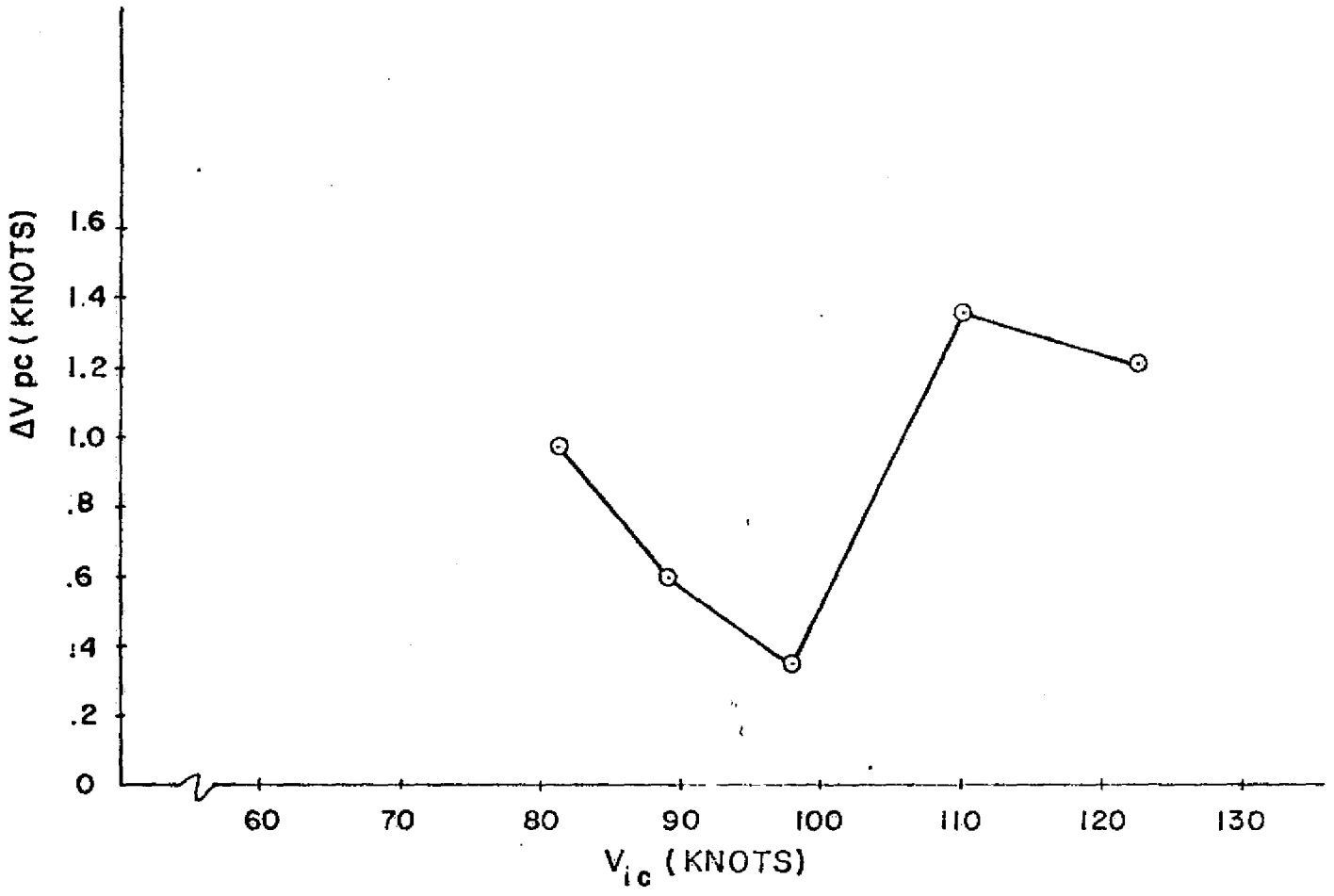

Figure 15. Airspeed Position Error Curve

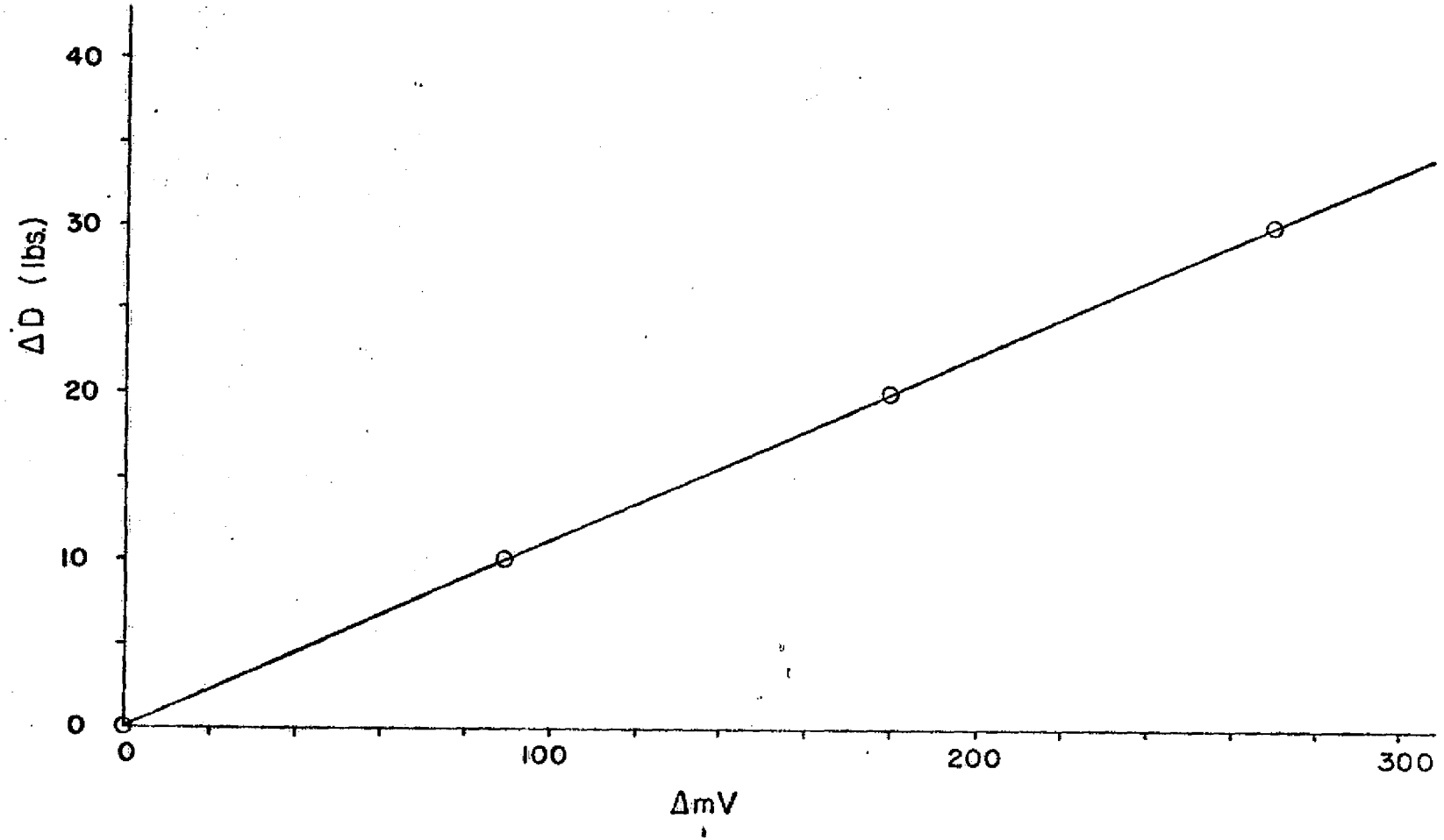

Figure 16. Load Cell Calibration Curve

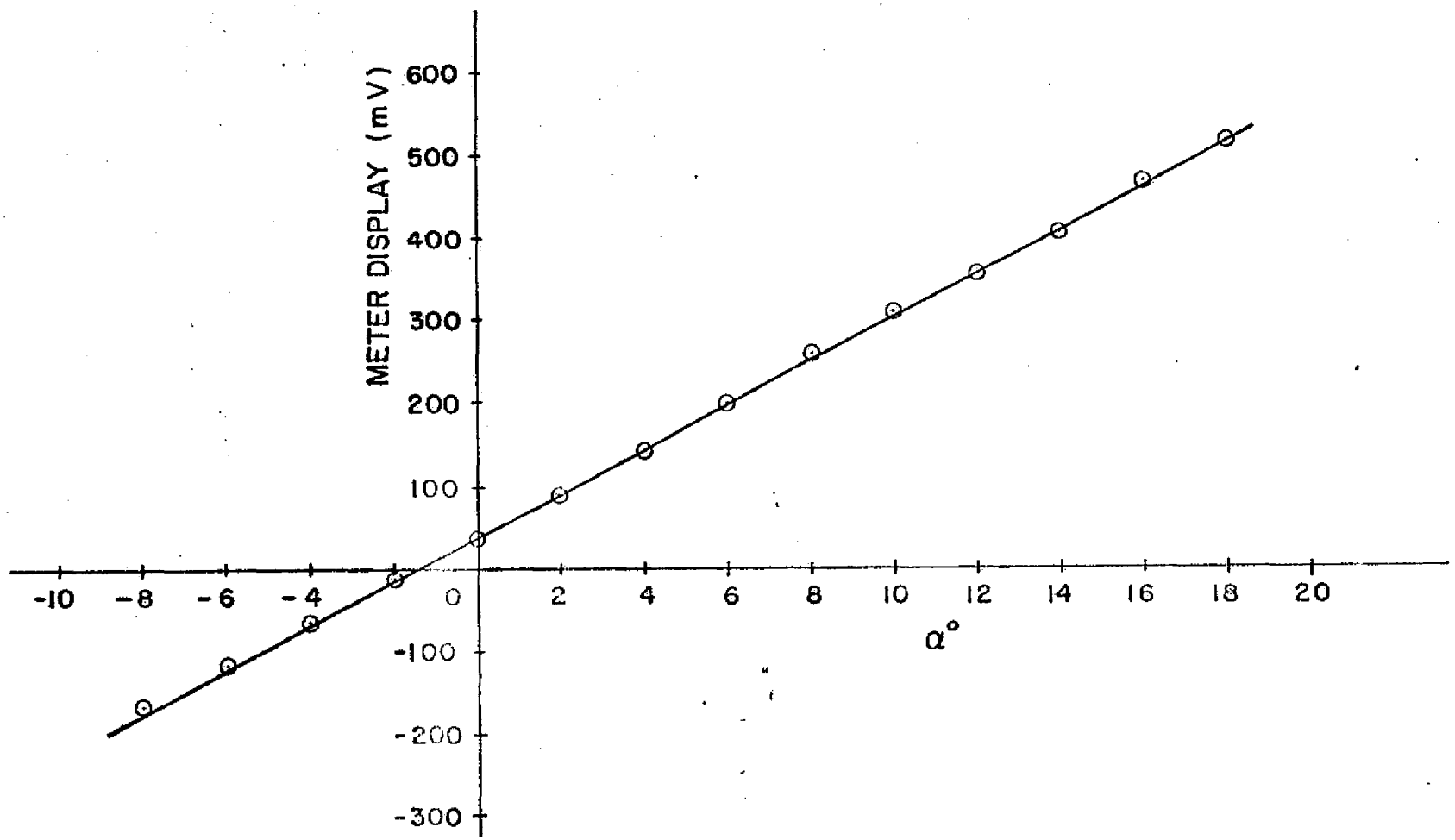

Figure 17. Angle of Attack Calibration Curve

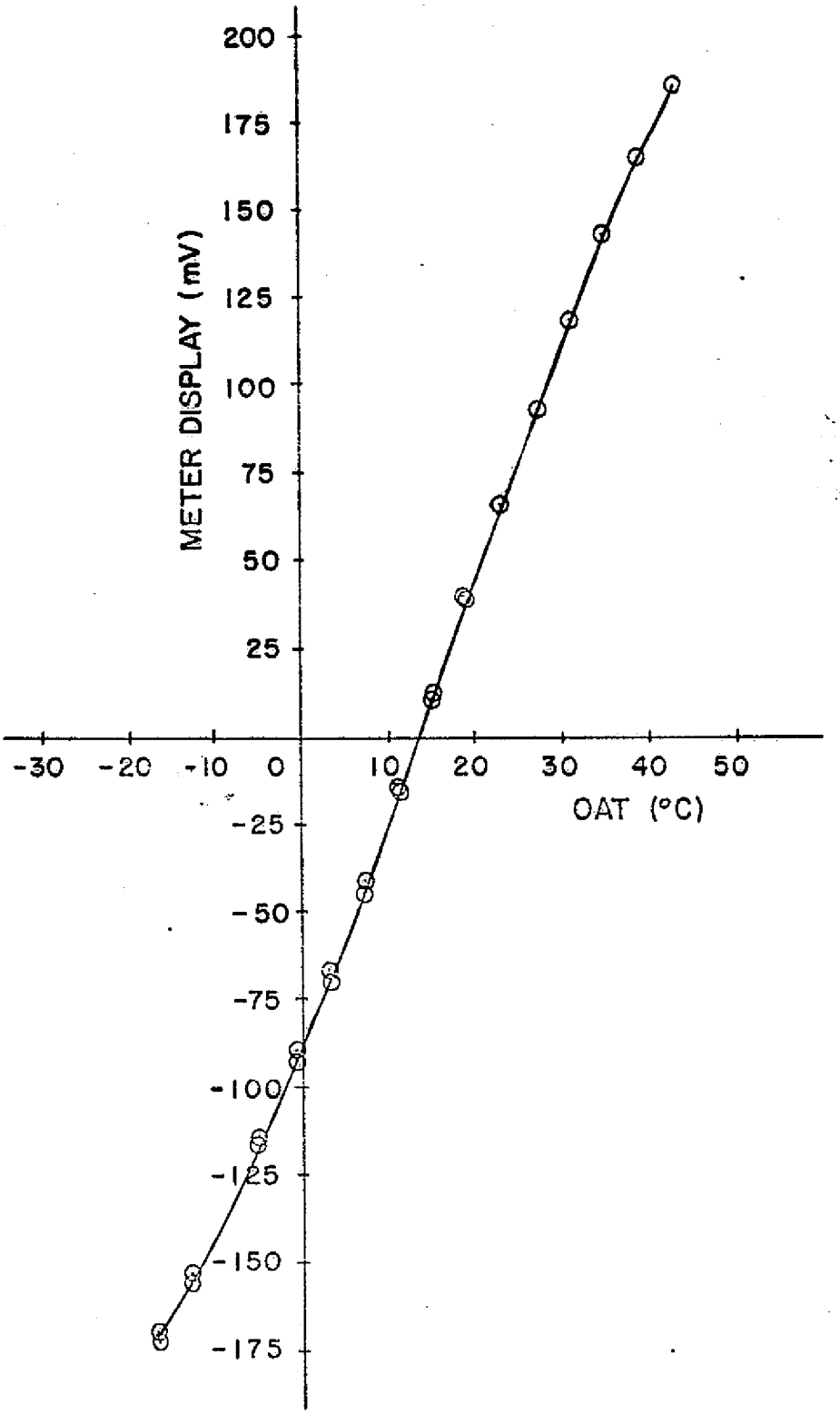

Figure 18. Outside Air Temperature Calibration Curve

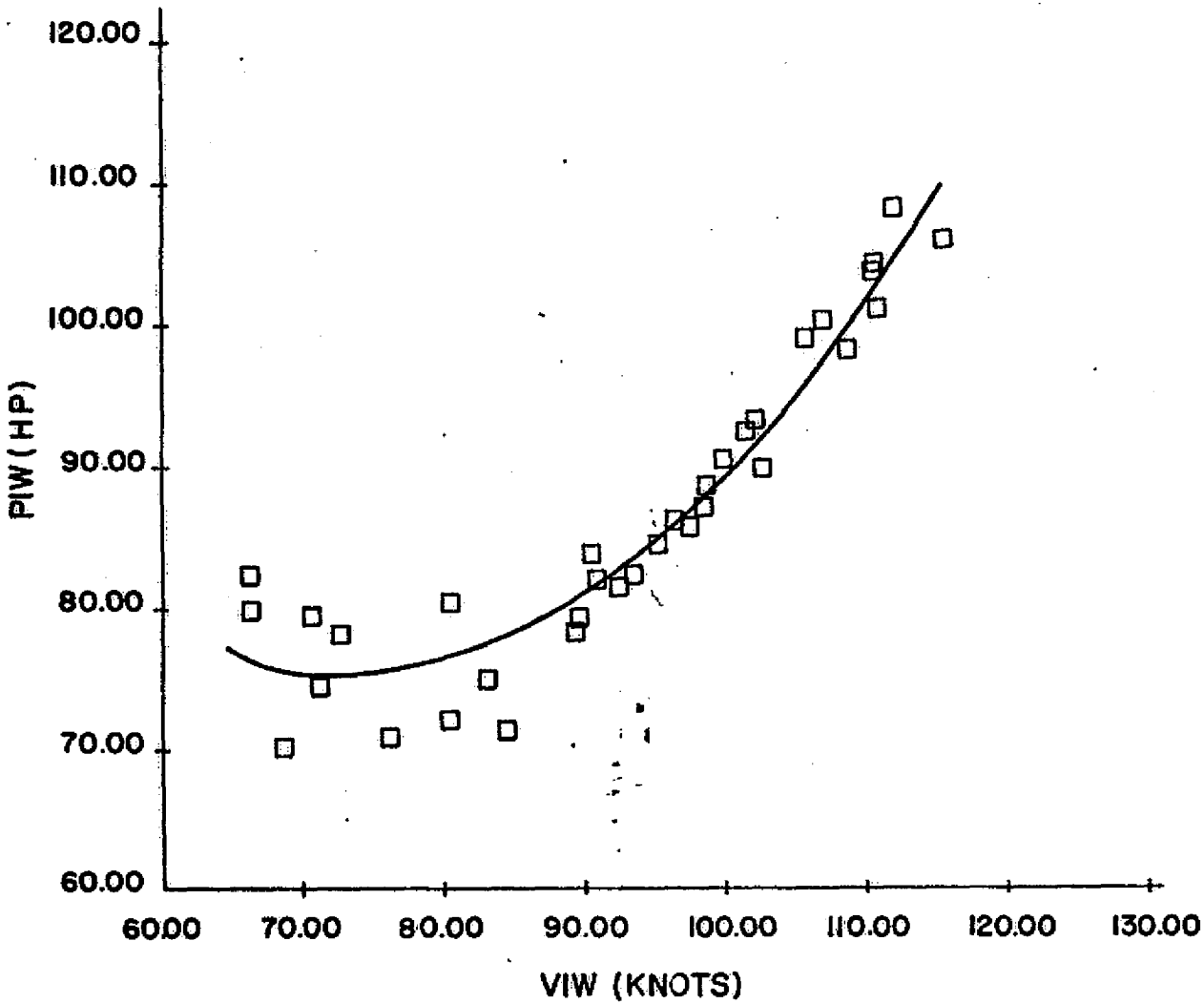

Figure 19. Power Required for Level Flight with No Drag Chute Attached

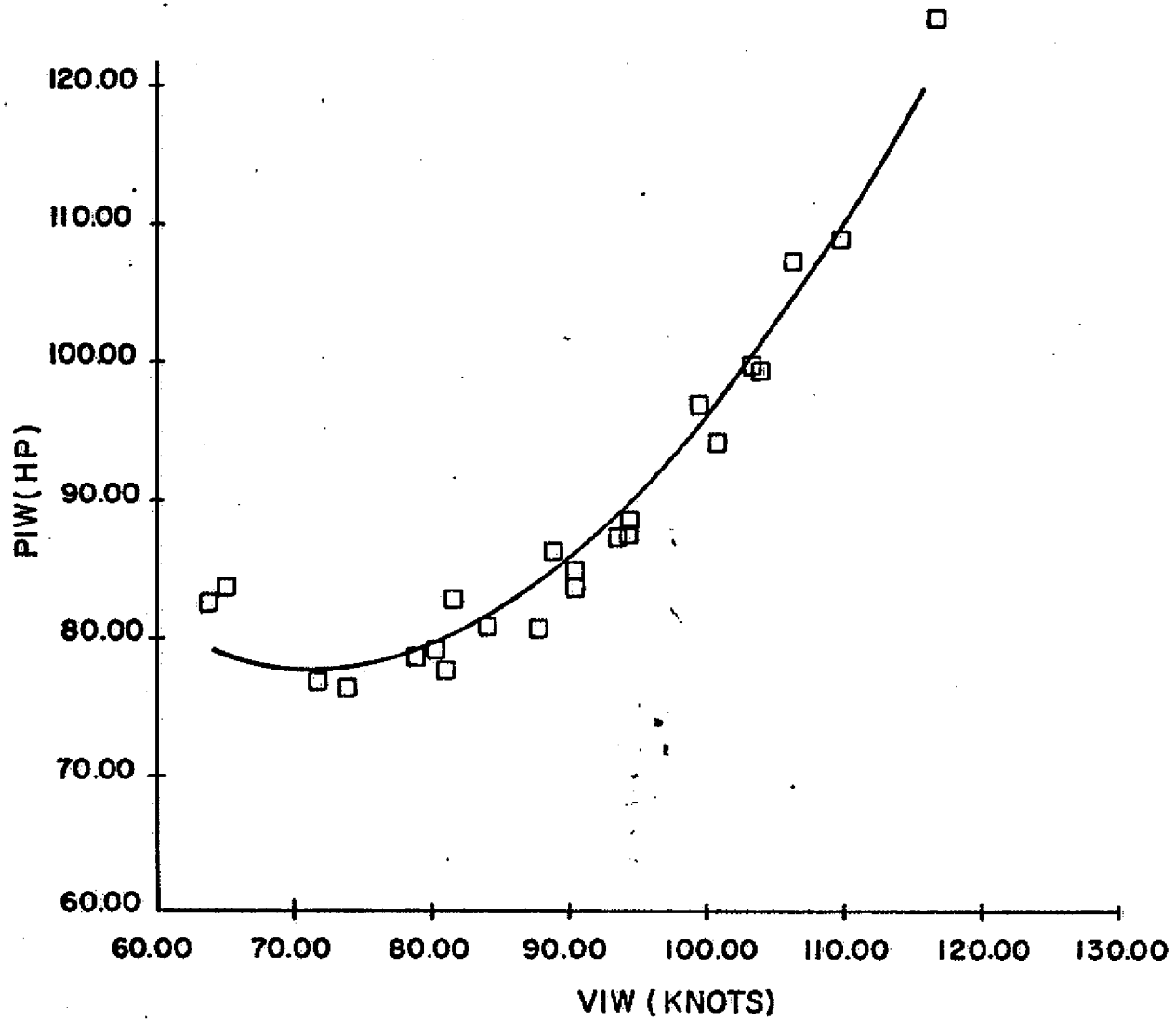

Figure 20. Power Required for Level Flight with Small Drag Chute Attached

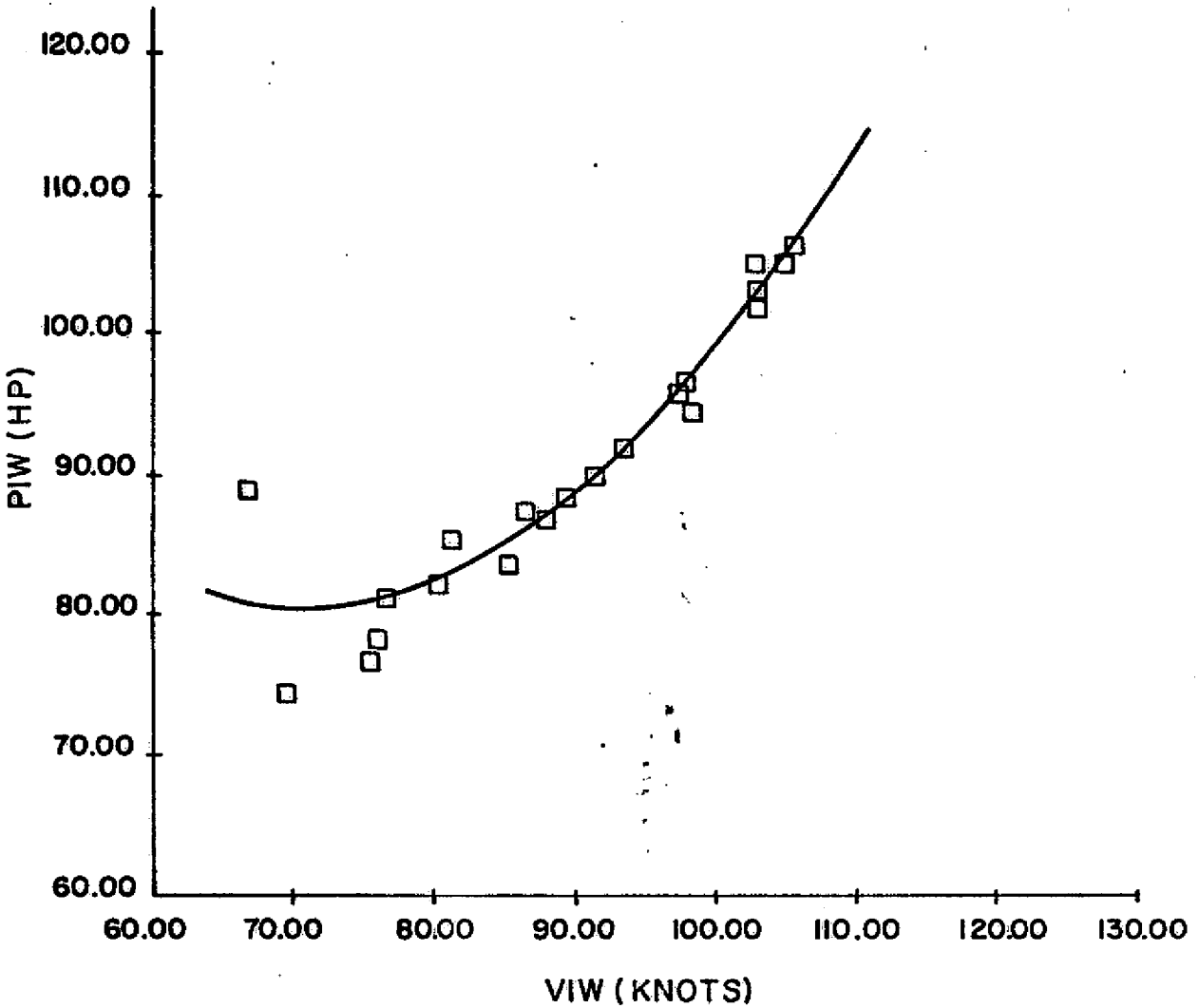

Figure 21. Power Required for Level Flight with Large Drag Chute Attached

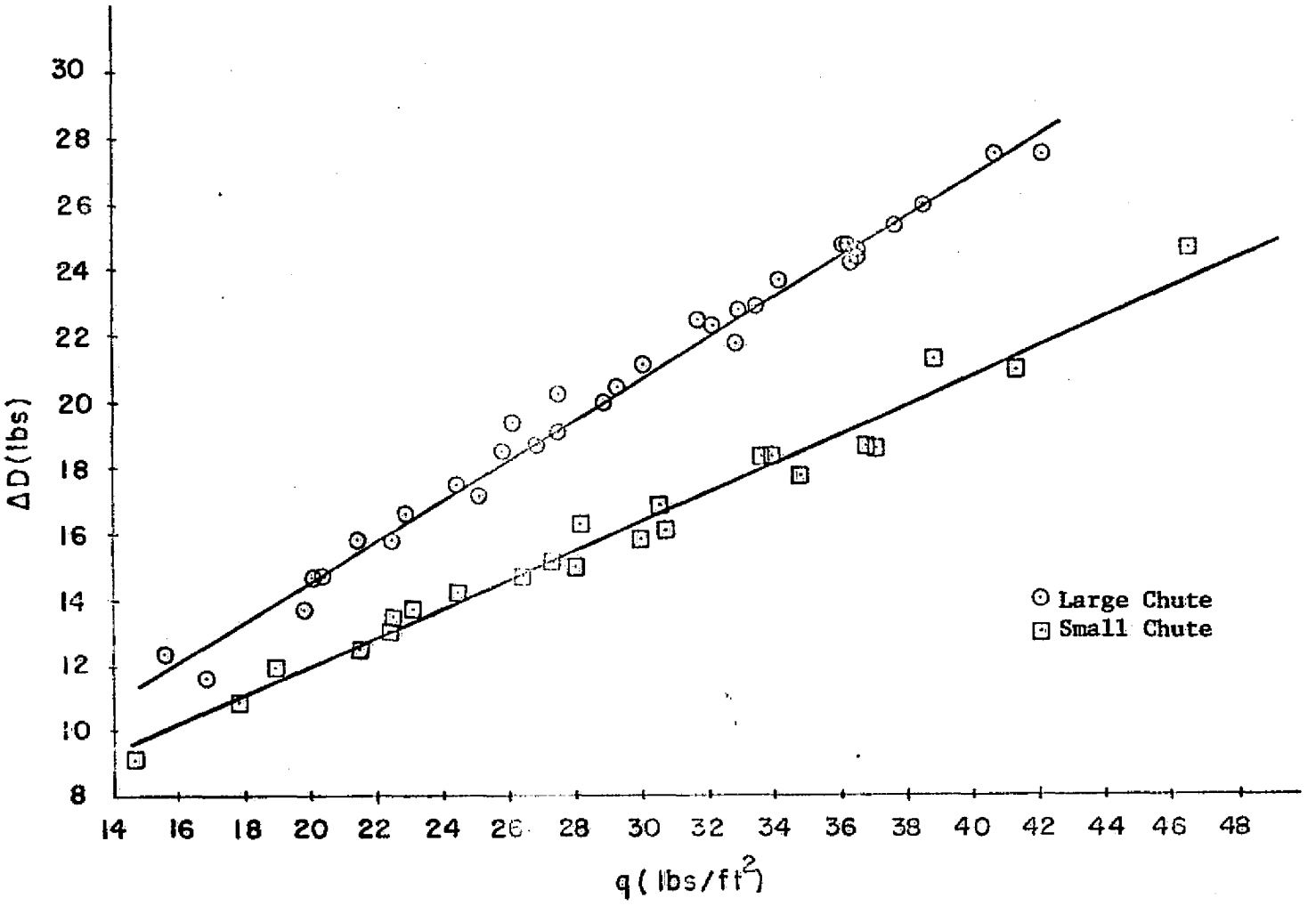

Figure 22. Chute Drag versus Dynamic Pressure

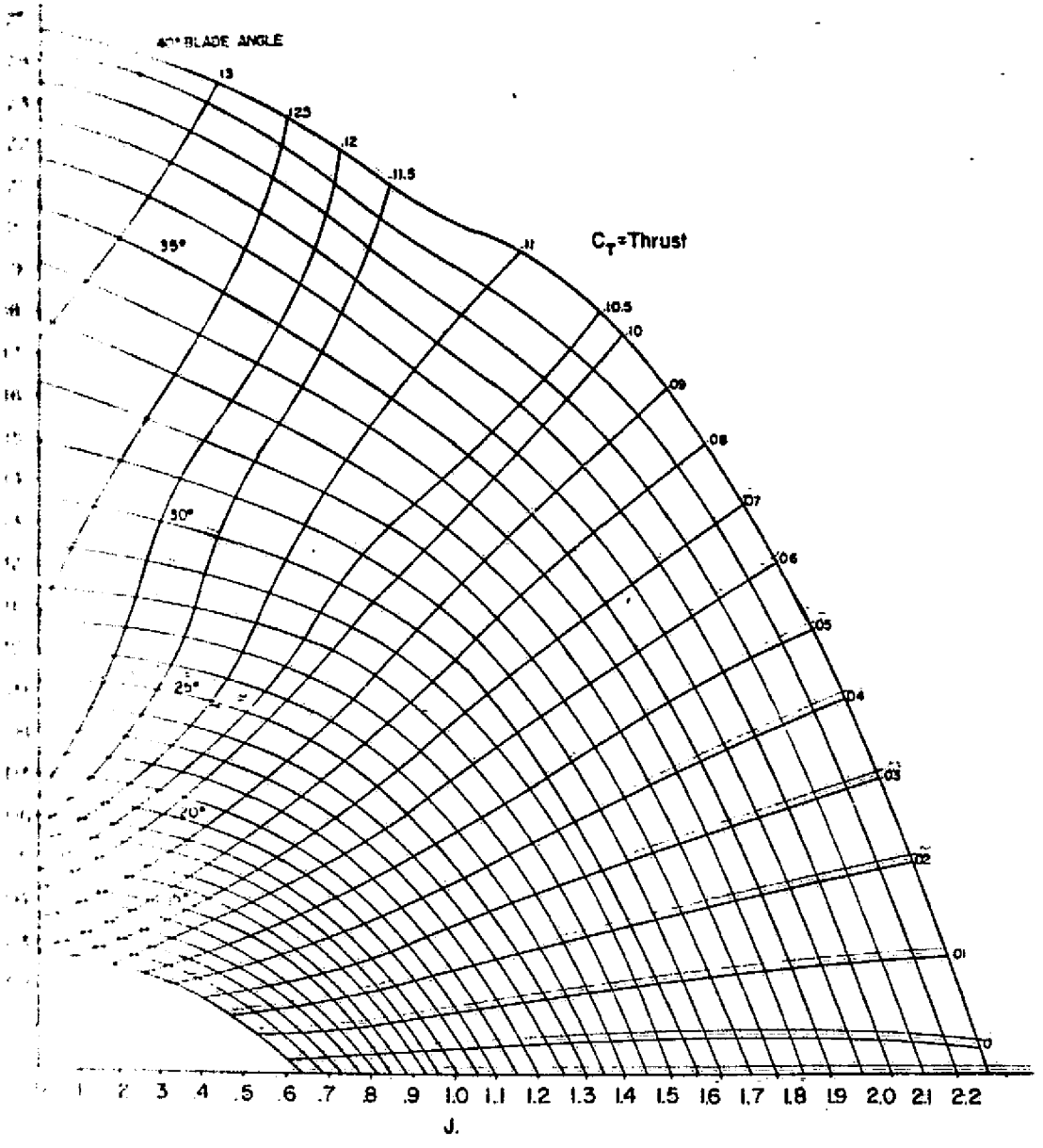

Figure 23. NACA Gray Chart. Coefficient of Power versus Advance Ratio

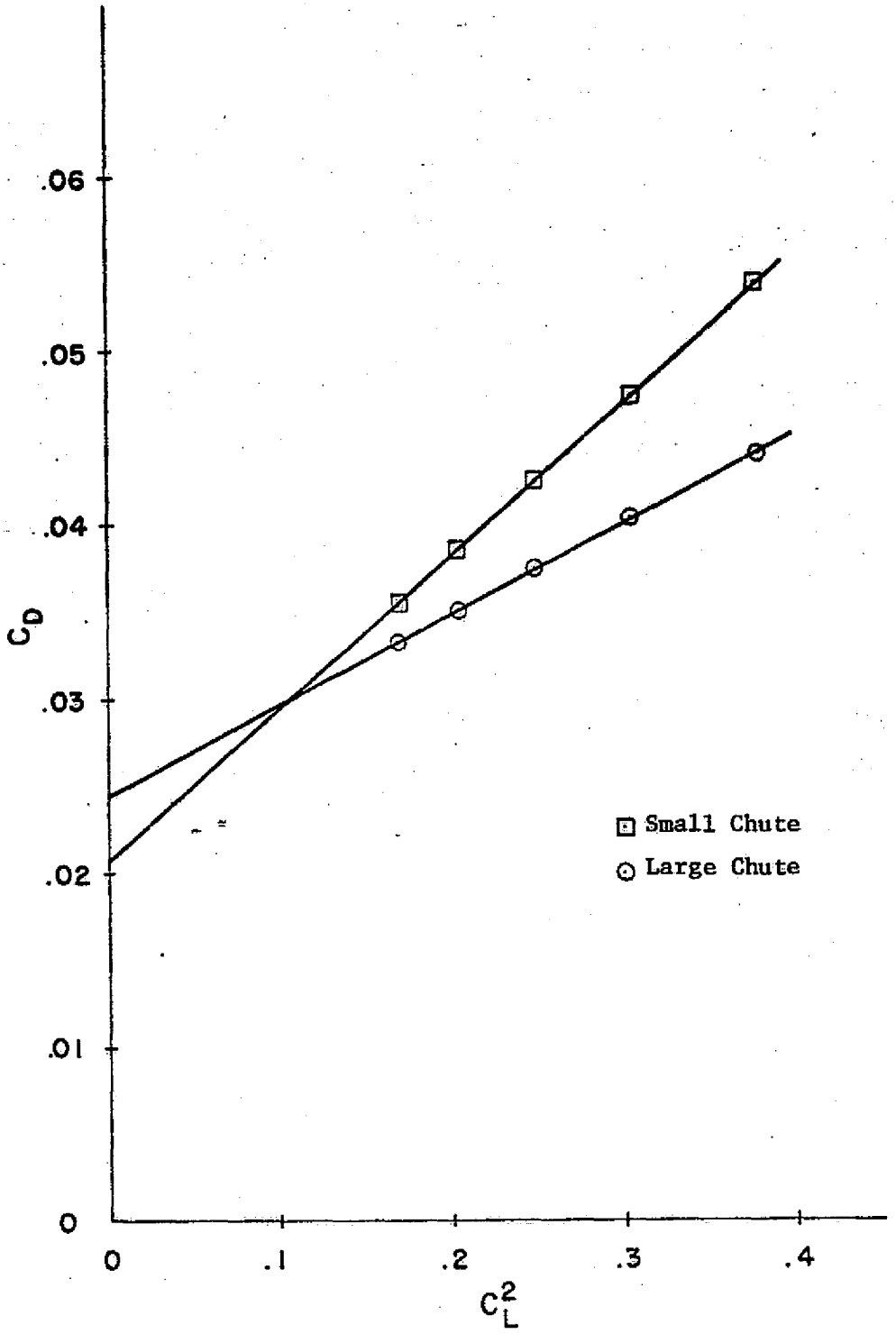

Figure 24. Coefficient of Drag versus Coefficient of Lift Squared. $E_p = 1.0$

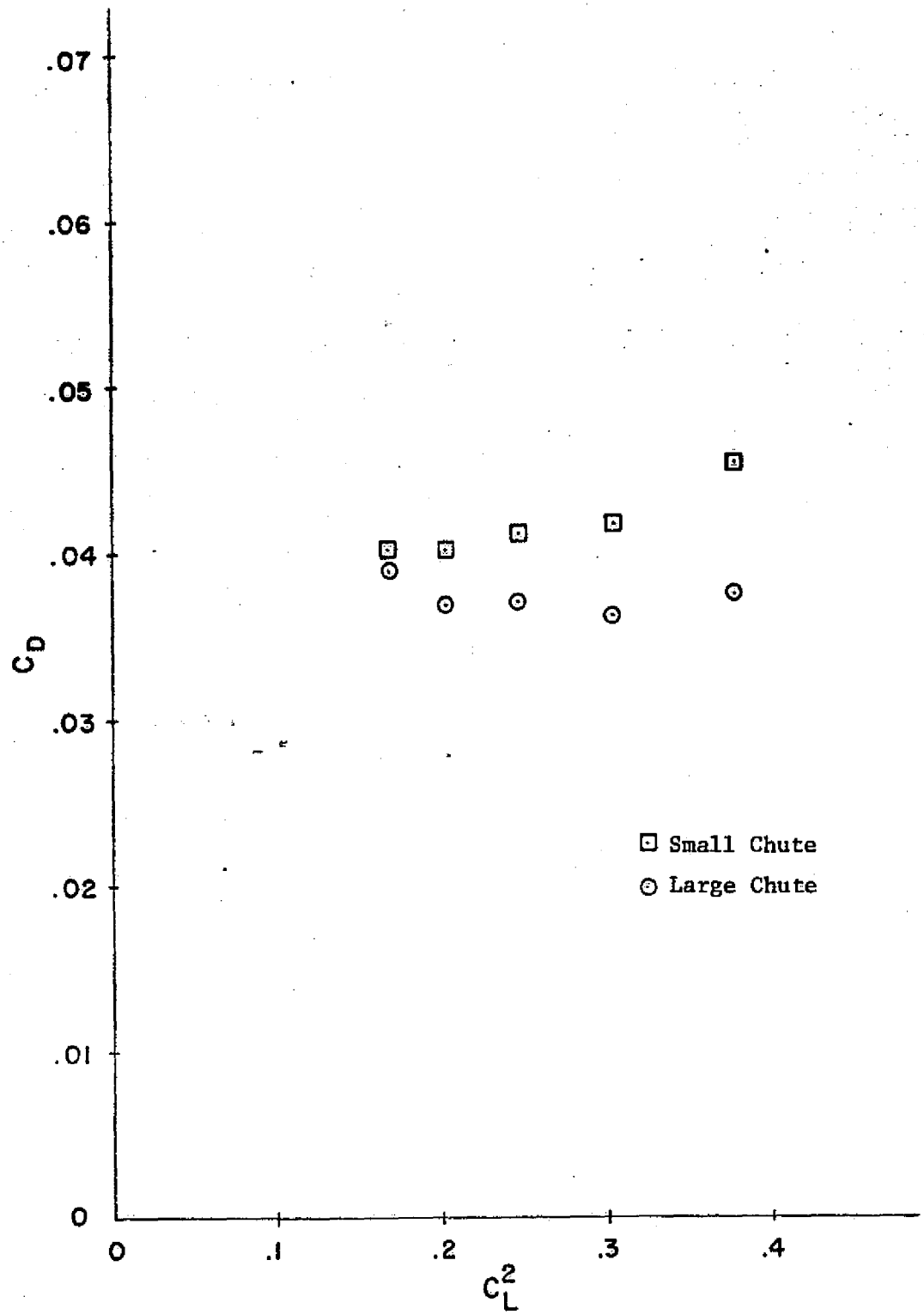

Figure 25. Coefficient of Drag versus Coefficient of Lift Squared. E_p Calculated from NASA CR2066

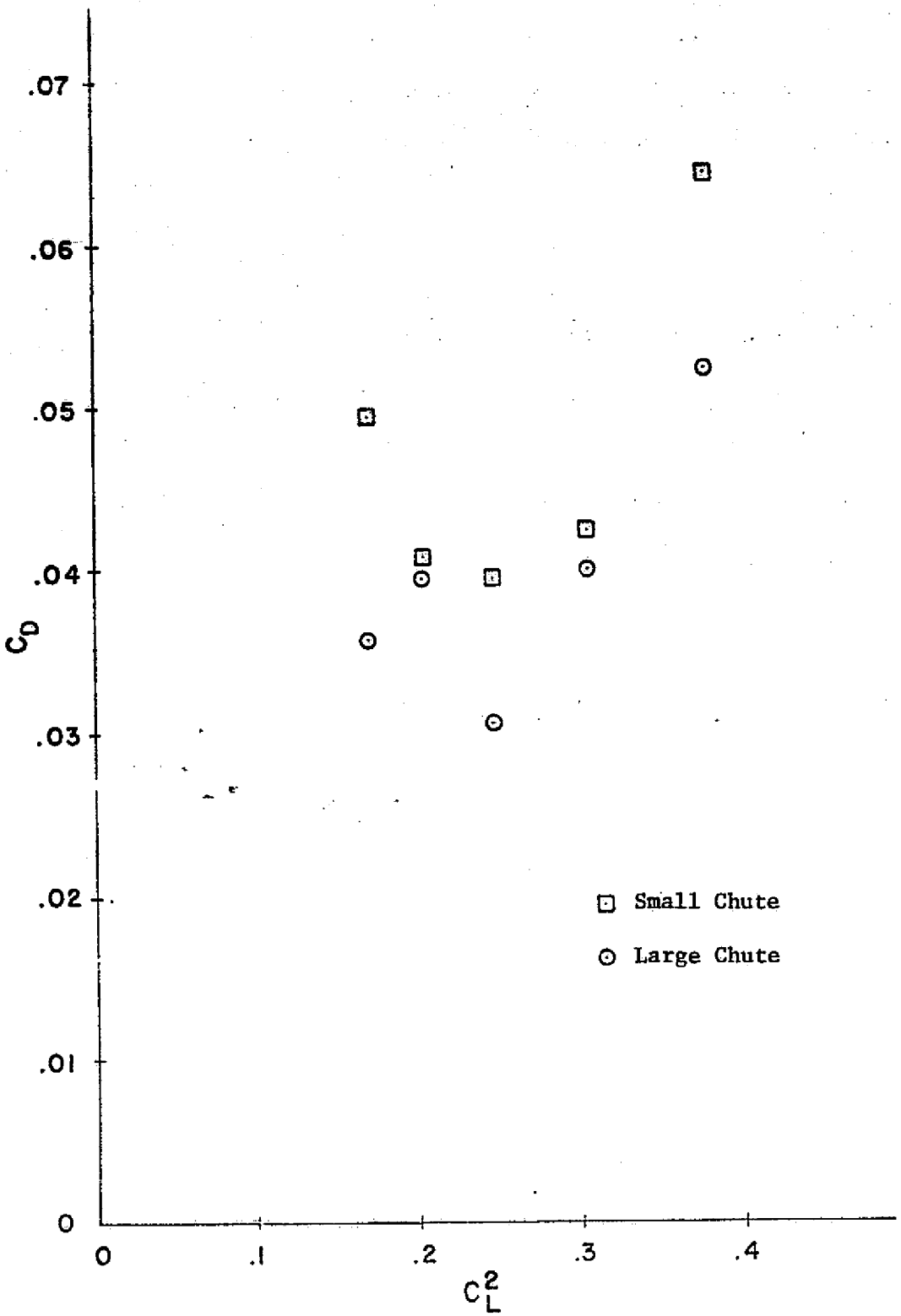

Figure 26. Coefficient of Drag versus Coefficient of Lift Squared. E_p Calculated from NACA Gray Chart

Table 1

Level Flight Performance

Configuration: Small Chute $E_p = 1.0$

$$P_1 = 4.8065 \times 10^{-5} V^3 + \frac{4139.61}{V}$$

$$P_2 = 5.4165 \times 10^{-5} V^3 + \frac{4164.95}{V}$$

$$\Delta D = 0.4425\ q + 3.161 = 1.500 \times 10^{-3} V^2 + 3.161$$

V (KTS)	P_1 (HP)	P_2 (HP)	ΔD (lbs)	D (lbs)	C_D	C_L^2	η_p
90	81.04	85.76	15.31	262.9	.0539	.378	.897
95	84.78	90.28	16.70	257.4	.0474	.305	.886
100	89.46	95.81	18.16	255.8	.0425	.248	.878
105	95.07	102.37	19.70	256.6	.0387	.204	.870
110	101.61	109.96	21.31	259.3	.0356	.170	.862

$$C_D = .0208 + .0876\ C_L^2$$

Table 2

Level Flight Performance

Configuration: Large Chute $E_P = 1.0$

$$P_1 = 4.8065 \times 10^{-5} V^3 + \frac{4139.61}{V}$$

$$P_2 = 5.5796 \times 10^{-5} V^3 + \frac{4283.19}{V}$$

$$\Delta D = .6149_q + 2.299 = 2.0844 \times 10^{-3} V^2 + 2.299$$

V (KTS)	P_1 (HP)	P_2 (HP)	ΔD (lbs)	D (lbs)	C_D	C_L^2	η_p
90	81.04	88.27	19.18	215.0	.0441	.378	.733
95	84.78	92.92	21.11	219.9	.0405	.305	.757
100	89.46	98.63	23.14	225.7	.0375	.248	.775
105	95.07	105.38	25.28	233.1	.0351	.204	.791
110	101.61	113.20	27.52	241.3	.0331	.170	.802

$$C_D = 0.0243 + .0528 C_L^2$$

Table 3

Level Flight Performance

Configuration: Small Chute E_p calculated by NASA CR2066

$$P_1 = 4.8065 \times 10^{-5} V^3 + \frac{4139.61}{V}$$

$$P_2 = 5.4165 \times 10^{-5} V^3 + \frac{4164.95}{V}$$

$$\Delta D = 0.4425\, q + 3.161 = 1.500 \times 10^{-3} V^2 + 3.161$$

V (KTS)	P_1 (HP)	P_2 (HP)	ΔD (lbs)	η_{P_1}	η_{P_2}	E_p	D (lbs)	C_D	C_L^2
90	81.04	85.76	15.31	.858	.867	1.010	222.4	.0456	.378
95	84.78	90.28	16.70	.881	.888	1.008	227.5	.0419	.305
100	89.46	95.81	18.16	.902	.904	1.002	248.3	.0413	.248
105	95.07	102.37	19.70	.915	.912	0.997	267.8	.0404	.204
110	101.61	109.96	21.31	.921	.913	0.991	294.2	.0404	.170

Table 4

Level Flight Performance

Configuration: Large Chute E_p calculated by NASA CR2066

$$P_1 = 4.8065 \times 10^{-5} V^3 + \frac{4139.61}{V}$$

$$P_2 = 5.5796 \times 10^{-5} V^3 + \frac{4283.19}{V}$$

$$\Delta D = .6149q + 2.299 = 2.0844 \times 10^{-3} V^2 + 2.299$$

V	P_1	P_2	ΔD	η_{P_1}	η_{P_2}	E_p	D	C_D	C_L^2
(KTS)	(HP)	(HP)	(LBS)				(LBS)		
90	81.04	88.27	19.18	.858	.870	1.014	183.6	.0377	.378
95	84.78	92.92	21.11	.881	.890	1.010	197.3	.0363	.305
100	89.46	98.63	23.14	.902	.903	1.001	223.3	.0371	.248
105	95.07	105.38	25.28	.915	.910	0.995	245.7	.0370	.204
110	101.61	113.20	27.52	.921	.909	0.987	276.4	.0379	.170

Table 5

Level Flight Performance

Configuration: Small Chute E_p calculated by NACA Gray Chart

$$P_1 = 4.8065 \times 10^{-5} V^3 + \frac{4139.61}{V}$$

$$P_2 = 5.4165 \times 10^{-5} V^3 + \frac{4164.95}{V}$$

$$\Delta D = 0.4425q + 3.161 = 1.500 \times 10^{-3} V^2 + 3.161$$

V (KTS)	P_1 (HP)	P_2 (HP)	ΔD (LBS)	η_{P_1}	η_{P_2}	E_p	D (LBS)	C_D	C_L^2
90	81.04	85.76	15.31	.866	.858	.911	314.3	.0644	.378
95	84.78	90.28	16.70	.874	.880	1.007	230.9	.0425	.305
100	89.46	95.81	18.16	.870	.874	1.005	237.9	.0395	.248
105	95.07	102.37	19.70	.902	.898	.996	271.8	.0409	.204
110	101.61	109.96	21.31	.896	.877	.979	358.4	.0492	.170

Table 6

Level Flight Performance

Configuration: Large Chute E_p calculated by NACA Gray Chart

$$P_1 = 4.8065 \times 10^{-5}V^3 + \frac{4139.61}{V}$$

$$P_2 = 5.5796 \times 10^{-5}V^3 + \frac{4283.19}{V}$$

$$\Delta D = .6149q + 2.299 = 2.0844 \times 10^{-3}V^2 + 2.299$$

V (KTS)	P_1 (HP)	P_2 (HP)	ΔD (LBS)	η_{P_1}	η_{P_2}	E_p	D (LBS)	C_D	C_L^2
90	81.04	88.27	19.18	.866	.855	.987	255.5	.0524	.378
95	84.78	92.92	21.11	.874	.875	1.001	217.4	.0400	.305
100	89.46	98.63	23.14	.870	.888	1.021	184.2	.0306	.248
105	95.07	105.38	25.28	.902	.892	.989	262.6	.0396	.204
110	101.61	113.20	27.52	.896	.890	.993	259.0	.0356	.170